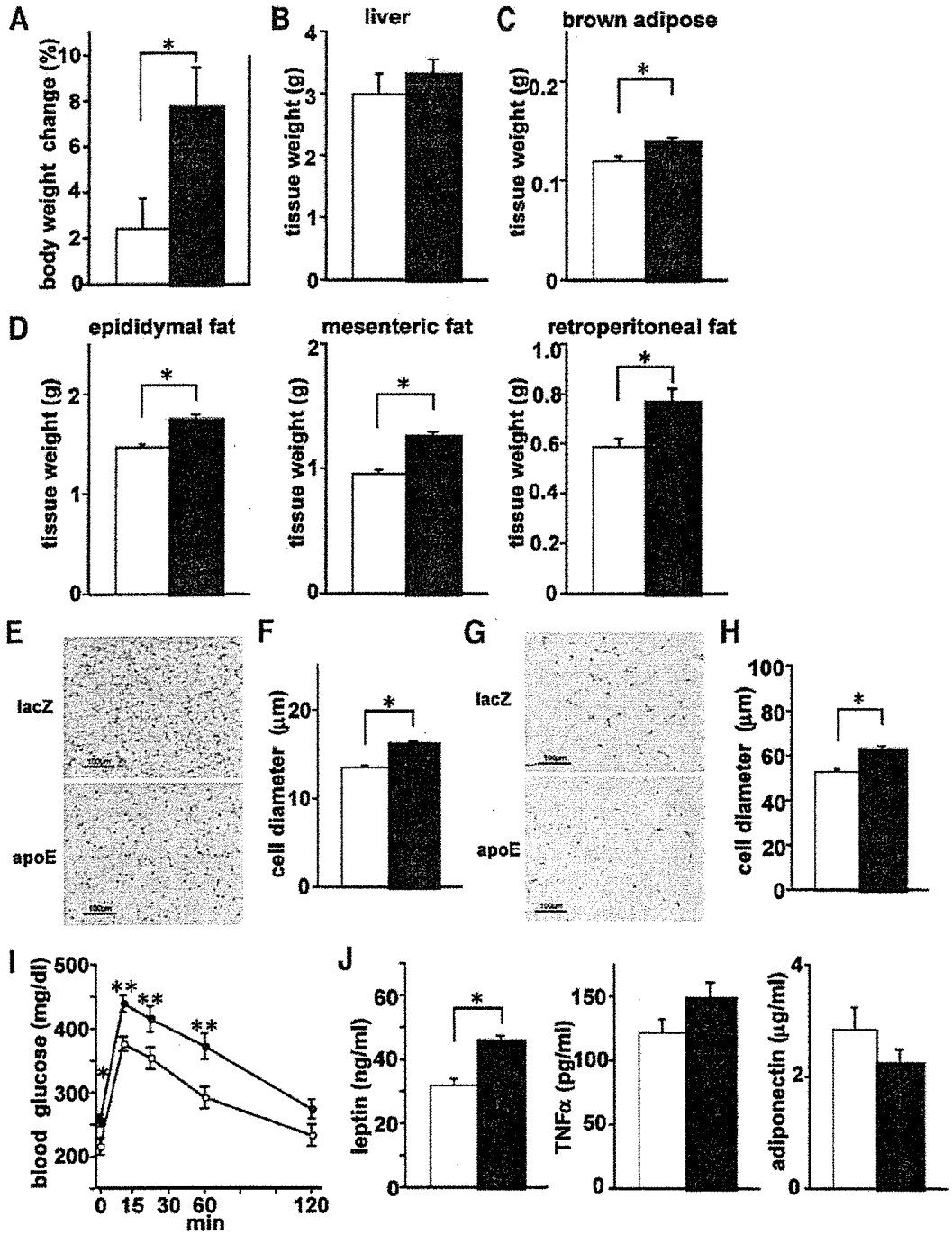

FIG. 4. Adenoviral apoE replenishment induced obesity and diabetes in genetically obese mice. ApoE$^{-/-}$;Ay/+ mice were intravenously administered LacZ (□ or ○) or apoE (■ or ●) adenovirus at 10 weeks of age after 4 weeks of high-fat loading. *A*: Body weight changes for 7 days after adenoviral administration were examined. *B–D*: Weights of the liver (*B*) and brown adipose (*C*) as well as white adipose (*D*: *left*, epididymal fat; *middle*, mesenteric fat; *right*, retroperitoneal fat) tissues were determined on day 7 after adenoviral injection (n = 6 per group). *E–H*: Histological findings of brown adipose (*E* and *F*) and mesenteric white adipose (*G* and *H*) tissues. Representative hematoxylin-eosin stained tissue samples are presented (*E* and *G*). Cell diameters were measured in these tissues (*F* and *H*). *I*: Glucose tolerance tests were performed on day 7 after adenoviral injection (n = 5–8 per group). *J*: Plasma adipocytokine levels (*left*, leptin; *middle*, TNF-α; *right*, adiponectin) were assayed on day 7 after adenoviral injection (n = 5–8 per group). Data are presented as means ± SE. *P < 0.05, **P < 0.01 by the unpaired t test.

that *ob/ob*;apoE$^{-/-}$ mice are also resistant to obesity. They attributed decreased adiposity in *ob/ob*;apoE$^{-/-}$ mice to impaired adipocyte differentiation based on in vitro findings that expression levels of aP2 and peroxisome proliferator–activated receptor-γ were markedly lower when bone marrow stromal cells and 3T3-L1 cells were cultured with apoE-less VLDL. However, in the present study, adipocytes in apoE$^{-/-}$;Ay/+ mice expressed these adipocyte-related proteins normally in vivo. Furthermore, apoE$^{-/-}$;Ay/+ mice showed better insulin sensitivity and less hepatic lipid accumulation, accompanied by improved adipocytokine profiles, than apoE$^{+/+}$;Ay/+ mice. Thus,

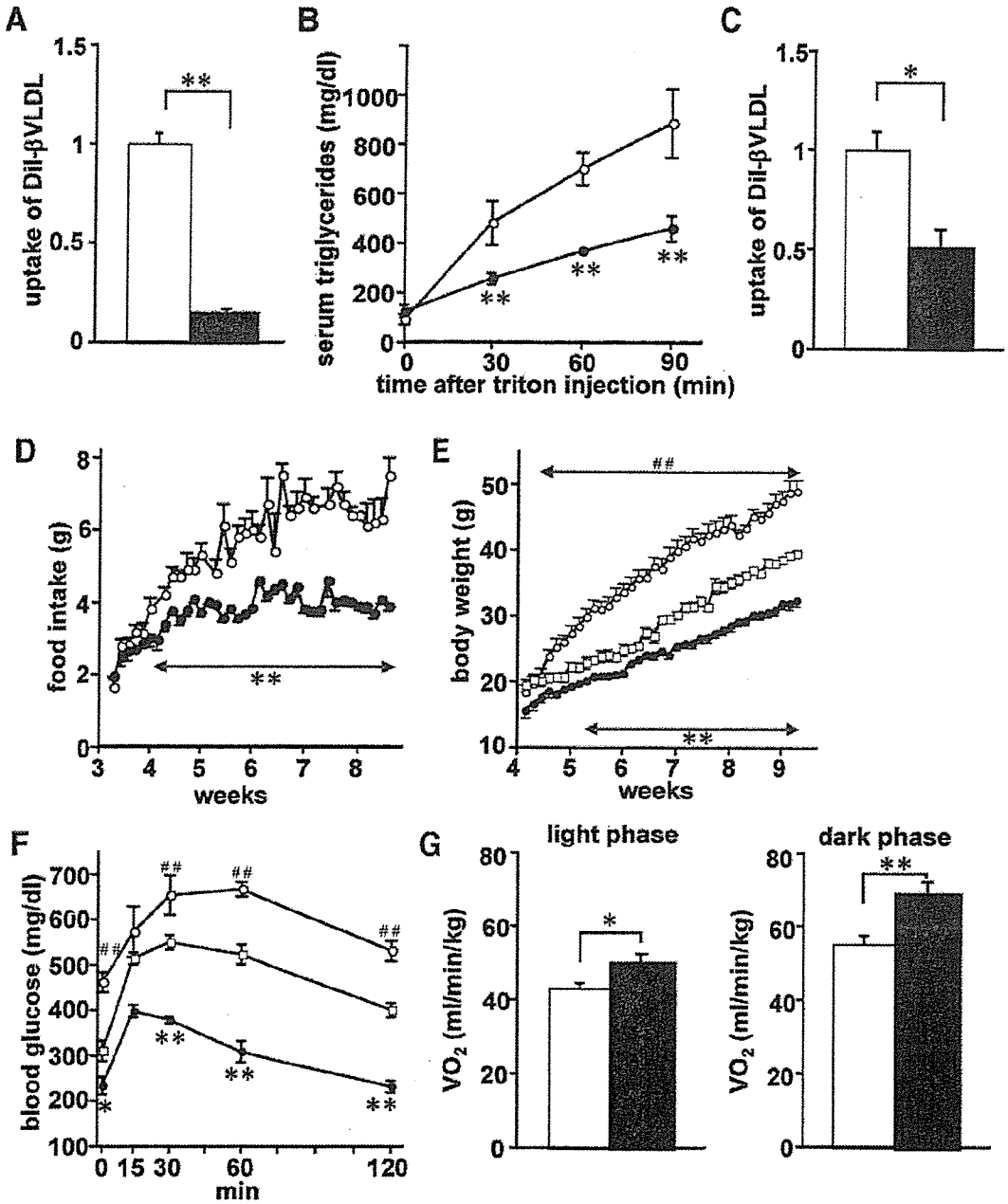

FIG. 5. ApoE deficiency inhibited β-VLDL uptake into adipocytes and the liver, decreased food intake, and increased energy expenditure. *A*: Uptakes of fluorescence-labeled β-VLDL, with (□) or without (■) apoE, into cultured adipocytes were measured. β-VLDL was isolated from apoE$^{-/-}$ mouse sera, followed by labeling with DiI and pretreatment with or without human recombinant apoE3. Fully differentiated 3T3-L1 adipocytes were incubated with apoE-positive or apoE-less β-VLDL for 8 h, followed by measurement of fluorescence uptake into adipocytes. Data are presented as the relative amounts of β-VLDL uptake compared with apoE-positive β-VLDL uptake (n = 6 per group). *B*: Triglyceride secretion rates from the liver after administration of Triton WR-1339 were measured in 11-week-old apoE$^{+/+}$;Ay/+ (○) and apoE$^{-/-}$;Ay/+ (●) mice fed a high-fat diet for 5 weeks. *C*: Hepatic uptake of β-VLDL with or without apoE. Fluorescence-labeled β-VLDL with or without apoE was intravenously injected into 11-week-old apoE$^{+/+}$;Ay/+ mice fed a high-fat diet for 5 weeks, followed by measurement of fluorescence levels in the liver 30 min after injection. Data are presented as the relative amounts of β-VLDL uptake compared with apoE-positive β-VLDL uptake (n = 4 per group). *D*: Daily food intake amounts from weaning through 8 weeks of age are presented. *E* and *F*: ApoE$^{+/+}$;Ay/+ mice were allotted into two groups at 4 weeks of age, and one group of apoE$^{+/+}$;Ay/+mice was given their daily food allotments based on the previous days' consumption by apoE$^{-/-}$;Ay/+ littermate mice. Body weights (*E*) were determined and glucose tolerance tests (*F*) were performed in apoE$^{+/+}$;Ay/+ mice (○), pair-fed apoE$^{+/+}$;Ay/+ mice (□), and apoE$^{-/-}$;Ay/+ mice (●) (n = 6–8 per group). *G*: Resting oxygen consumption in the light and dark phases was measured at 5 weeks of age with open-circuit indirect calorimetry. n = 4 per group. Data are presented as means ± SE. *P < 0.05, **P < 0.01 by the unpaired t test. In *E* and *F* ##P < 0.01 for pair-feeding apoE$^{+/+}$;Ay/+ mice versus apoE$^{+/+}$;Ay/+ mice; *P < 0.05, **P < 0.01 for pair-feeding apoE$^{+/+}$;Ay/+ mice versus apoE$^{-/-}$;Ay/+ mice, by one-way ANOVA.

decreased adiposity and improved insulin sensitivity in apoE$^{-/-}$;Ay/+ mice can be explained by factors other than adipocyte differentiation.

While body weight and adiposity were similar in young apoE$^{-/-}$ and apoE$^{+/+}$ mice, apoE deficiency ameliorated obesity and insulin resistance under obesity-inducing con-

ditions, such as aging, genetic susceptibility, and dietary loading, suggesting that apoE is involved in obesity development, i.e., excess fat accumulation, while being less involved in basal fat accumulation. Lack of apoE in β-VLDL markedly impaired β-VLDL transport into adipocytes. ApoE is an important component of VLDL. There are several receptors, including VLDL receptor (VLDLR) and LDL receptor–related protein, which recognize VLDL in an apoE-dependent manner (22). Among them, VLDLRs reportedly have similar affinities for apoE2, -E3, and -E4 isoforms (29). In addition, VLDLR-deficient mice reportedly exhibit obesity resistance with high-fat chow loading (30). Taken together with our findings that replenishment of apoE2, -E3, and -E4 isoforms contributes similarly to fat accumulation and glucose tolerance in apoE$^{-/-}$;Ay/+ mice, the apoE-VLDLR interaction plays an important role in the development of obesity. Furthermore, it is well known that high levels of plasma VLDL are associated with obesity and type 2 diabetes (31). Thus, receptor-mediated VLDL transport into adipocytes in an apoE-dependent manner is involved mainly in excess lipid uptake into adipocytes. Lipid uptake, required for adipocyte differentiation and metabolic activities, might be mediated mainly by apoE-independent lipid transport pathways or de novo lipid synthesis in adipocytes.

In addition, transport of apoE-deficient β-VLDL into the liver was markedly impaired compared with that of apoE-positive β-VLDL. Despite decreased triglyceride secretion, apoE deficiency decreased hepatic fat accumulation in Ay, but not in wild-type, mice (11). Hepatic expressions of SREBP1c and fatty acid synthase were similar in apoE$^{-/-}$;Ay/+ and apoE$^{+/+}$;Ay/+ mice (data not shown), suggesting no apparent decrease in hepatic fatty acid synthesis in apoE$^{-/-}$;Ay/+ mice. These findings suggest that apoE-dependent uptake of β-VLDL into hepatocytes is involved in the development of hepatic steatosis in Ay mice. The machinery that transports β-VLDL into the liver, including the receptor(s) playing a major role, is a potential target for elucidating the mechanism underlying hepatic steatosis.

Intriguingly, in apoE$^{-/-}$;Ay/+ mice, food intake was decreased and energy expenditure enhanced compared with apoE$^{+/+}$;Ay/+ mice. Pair-feeding experiments revealed that both these phenomena result in obesity resistance in apoE$^{-/-}$;Ay/+ mice. There appear to be several possible explanations for these alterations in energy metabolism. First, hyperlipidemia induced by apoE deficiency might contribute to decreased food intake and increased energy expenditure. However, LDLR$^{-/-}$ mice, which also exhibit hyperlipidemia, reportedly become more obese and diabetic in response to high-fat and high-carbonate diets than wild-type mice (13). In addition, food intake was similar in LDLR$^{-/-}$ mice and LDLR$^{+/+}$ mice (13). Therefore, although hyperlipidemia is more severe in apoE$^{-/-}$ than in LDLR$^{-/-}$ mice, involvement of hyperlipidemia in food intake regulation might be unlikely in our model. Second, we speculate that leptin sensitization is involved in decreased food intake and increased energy expenditure. Obesity is well known to be associated with poor responses to leptin despite hyperleptinemia, a state defined as leptin resistance (32). Lower plasma leptin levels with lower body weight in apoE$^{-/-}$;Ay/+ mice compared with apoE$^{+/+}$;Ay/+ mice suggests greater leptin sentivity in the former. Therefore, decreased food intake and increased energy expenditure in apoE$^{-/-}$;Ay/+ mice might be explained by leptin sensitization. We have recently reported that alterations in metabolism in adipose tissue affect food intake amounts (19). However, *ob/ob*;apoE$^{-/-}$ mice are also reportedly resistant to obesity (14). Since *ob/ob* mice are leptin deficient, the obesity resistance in *ob/ob*;apoE$^{-/-}$ mice is not mediated by leptin signaling, e.g., leptin sensitization, although food intake and energy expenditure were not measured in the earlier study (14). Thus, mechanisms other than leptin sensitization might be involved in decreased food intake and increased energy expenditure in apoE$^{-/-}$;Ay/+ mice. Third, direct effects of apoE on neurons are also possible. ApoE, produced by glial cells, is a major apolipoprotein in the brain and mediates the transport of cholesterol and phospholipids, and its receptors are abundantly expressed on neurons (33). Furthermore, numerous studies have shown that apoE plays multiple roles in the nervous system. In the central and peripheral nervous systems, apoE promotes neurite outgrowth and regeneration (34). ApoE protects neurons from oxidative injury (35) and modulates amyloid-β deposition (36), interactions with Alzheimer amyloid precursor protein (37), and transmission of signals to neurons (38). In this context, modulation of neurons by apoE might be involved in energy metabolism. ApoE is reportedly expressed in tissues other than the liver, including the brain (33) and adipose tissue (39). ApoE deficiency in these tissues may affect the metabolic phenotypes of apoE$^{-/-}$;Ay/+ mice observed herein. Intensive research, including tissue-specific disruption of apoE or its receptor, is required to examine this hypothesis.

ApoE is involved in surplus fat accumulation and energy metabolism, including regulation of food intake and energy expenditure. Thus, excess fat accumulation via an apoE-dependent pathway might play a role in development of the metabolic syndrome. In addition to dissipation of surplus energy (4), apoE-dependent excess lipid transport is a potentially novel therapeutic target for the metabolic syndrome.

ACKNOWLEDGMENTS

This work was supported by a Grant-in-Aid for Scientific Research (B2, 15390282) to H.K.; a Grant-in-Aid for Scientific Research (17790599) to Y.I. from the Ministry of Education, Science, Sports and Culture of Japan; and a Grant-in-Aid for Scientific Research (H16-genome-003) to Y.O. from the Ministry of Health, Labor and Welfare of Japan. This work was also supported by the 21st Century COE Programs "CRESCENDO" to H.K. and "the Center for Innovative Therapeutic Development for Common Diseases" to Y.O. from the Ministry of Education Science, Sports and Culture.

We thank I. Sato, J. Fushimi, K. Kawamura, and M. Hoshi for technical support.

REFERENCES

1. Eckel RH, Grundy SM, Zimmet PZ: The metabolic syndrome. *Lancet* 365:1415–1428, 2005
2. Fruhbeck G, Gomez-Ambrosi J: Control of body weight: a physiologic and transgenic perspective. *Diabetologia* 46:143–172, 2003
3. Friedman JM: A war on obesity, not the obese. *Science* 299:856–858, 2003
4. Ishigaki Y, Katagiri H, Yamada T, Ogihara T, Imai J, Uno K, Hasegawa Y, Gao J, Ishihara H, Shimosegawa T, Sakoda H, Asano T, Oka Y: Dissipating excess energy stored in the liver is a potential treatment strategy for diabetes associated with obesity. *Diabetes* 54:322–332, 2005
5. Moitra J, Mason MM, Olive M, Krylov D, Gavrilova O, Marcus-Samuels B, Feigenbaum L, Lee E, Aoyama T, Eckhaus M, Reitman ML, Vinson C: Life without white fat: a transgenic mouse. *Genes Dev* 12:3168–3181, 1998
6. Shimomura I, Hammer RE, Richardson JA, Ikemoto S, Bashmakov Y,

Goldstein JL, Brown MS: Insulin resistance and diabetes mellitus in transgenic mice expressing nuclear SREBP-1c in adipose tissue: model for congenital generalized lipodystrophy. *Genes Dev* 12:3182–3194, 1998
7. Oral EA, Simha V, Ruiz E, Andewelt A, Premkumar A, Snell P, Wagner AJ, DePaoli AM, Reitman ML, Taylor SI, Gorden P, Garg A: Leptin-replacement therapy for lipodystrophy. *N Engl J Med* 346:570–578, 2002
8. Hussain MM, Maxfield FR, Mas-Oliva J, Tabas I, Ji ZS, Innerarity TL, Mahley RW: Clearance of chylomicron remnants by the low density lipoprotein receptor-related protein/alpha 2-macroglobulin receptor. *J Biol Chem* 266:13936–13940, 1991
9. Chappell DA, Medh JD: Receptor-mediated mechanisms of lipoprotein remnant catabolism. *Prog Lipid Res* 37:393–422, 1998
10. Cooper AD: Hepatic uptake of chylomicron remnants. *J Lipid Res* 38:2173–2192, 1997
11. Kuipers F, Jong MC, Lin Y, Eck M, Havinga R, Bloks V, Verkade HJ, Hofker MH, Moshage H, Berkel TJ, Vonk RJ, Havekes LM: Impaired secretion of very low density lipoprotein-triglycerides by apolipoprotein E-deficient mouse hepatocytes. *J Clin Invest* 100:2915–2922, 1997
12. Lyngdorf LG, Gregersen S, Daugherty A, Falk E: Paradoxical reduction of atherosclerosis in apoE-deficient mice with obesity-related type 2 diabetes. *Cardiovasc Res* 59:854–862, 2003
13. Schreyer SA, Vick C, Lystig TC, Mystkowski P, LeBoeuf RC: LDL receptor but not apolipoprotein E deficiency increases diet-induced obesity and diabetes in mice. *Am J Physiol Endocrinol Metab* 282:E207–E214, 2002
14. Chiba T, Nakazawa T, Yui K, Kaneko E, Shimokado K: VLDL induces adipocyte differentiation in ApoE-dependent manner. *Arterioscler Thromb Vasc Biol* 23:1423–1429, 2003
15. Zhang SH, Reddick RL, Piedrahita JA, Maeda N: Spontaneous hypercholesterolemia and arterial lesions in mice lacking apolipoprotein E. *Science* 258:468–471, 1992
16. Ishigaki Y, Oikawa S, Suzuki T, Usui S, Magoori K, Kim DH, Suzuki H, Sasaki J, Sasano H, Okazaki M, Toyota T, Saito T, Yamamoto TT: Virus-mediated transduction of apolipoprotein E (ApoE)-sendai develops lipoprotein glomerulopathy in ApoE-deficient mice. *J Biol Chem* 275: 31269–31273, 2000
17. Anai M, Funaki M, Ogihara T, Terasaki J, Inukai K, Katagiri H, Fukushima Y, Yazaki Y, Kikuchi M, Oka Y, Asano T: Altered expression levels and impaired steps in the pathway to phosphatidylinositol 3-kinase activation via insulin receptor substrates 1 and 2 in Zucker fatty rats. *Diabetes* 47:13–23, 1998
18. Usui S, Hara Y, Hosaki S, Okazaki M: A new on-line dual enzymatic method for simultaneous quantification of cholesterol and triglycerides in lipoproteins by HPLC. *J Lipid Res* 43:805–814, 2002
19. Yamada T, Katagiri H, Ishigaki Y, Ogihara T, Imai J, Uno K, Hasegawa Y, Gao J, Ishihara H, Niijima A, Mano H, Aburatani H, Asano T, Oka Y: Signals from intra-abdominal fat modulate insulin and leptin sensitivity through different mechanisms: neuronal involvement in food-intake regulation. *Cell Metab* 3:223–229, 2006
20. Uno K, Katagiri H, Yamada T, Ishigaki Y, Ogihara T, Imai J, Hasegawa Y, Gao J, Kaneko K, Iwasaki H, Ishihara H, Sasano H, Inukai K, Mizuguchi H, Asano T, Shiota M, Nakazato M, Oka Y: Neuronal pathway from the liver modulates energy expenditure and systemic insulin sensitivity. *Science* 312:1656–1659, 2006
21. Min J, Okada S, Kanzaki M, Elmendorf JS, Coker KJ, Ceresa BP, Syu LJ, Noda Y, Saltiel AR, Pessin JE: Synip: a novel insulin-regulated syntaxin 4-binding protein mediating GLUT4 translocation in adipocytes. *Mol Cell* 3:751–760, 1999
22. Takahashi S, Kawarabayasi Y, Nakai T, Sakai J, Yamamoto T: Rabbit very low density lipoprotein receptor: a low density lipoprotein receptor-like protein with distinct ligand specificity. *Proc Natl Acad Sci U S A* 89:9252–9256, 1992
23. Descamps O, Bilheimer D, Herz J: Insulin stimulates receptor-mediated uptake of apoE-enriched lipoproteins and activated alpha 2-macroglobulin in adipocytes. *J Biol Chem* 268:974–981, 1993
24. Wilsie LC, Chanchani S, Navaratna D, Orlando RA: Cell surface heparan sulfate proteoglycans contribute to intracellular lipid accumulation in adipocytes. *Lipids Health Dis* 4:2, 2005
25. Siri P, Candela N, Zhang YL, Ko C, Eusufzai S, Ginsberg HN, Huang LS: Post-transcriptional stimulation of the assembly and secretion of triglyceride-rich apolipoprotein B lipoproteins in a mouse with selective deficiency of brown adipose tissue, obesity, and insulin resistance. *J Biol Chem* 276:46064–46072, 2001
26. Fujino T, Asaba H, Kang MJ, Ikeda Y, Sone H, Takada S, Kim DH, Ioka RX, Ono M, Tomoyori H, Okubo M, Murase T, Kamataki A, Yamamoto J, Magoori K, Takahashi S, Miyamoto Y, Oishi H, Nose M, Okazaki M, Usui S, Imaizumi K, Yanagisawa M, Sakai J, Yamamoto TT: Low-density lipoprotein receptor-related protein 5 (LRP5) is essential for normal cholesterol metabolism and glucose-induced insulin secretion. *Proc Natl Acad Sci U S A* 100:229–234, 2003
27. Xu H, Barnes GT, Yang Q, Tan G, Yang D, Chou CJ, Sole J, Nichols A, Ross JS, Tartaglia LA, Chen H: Chronic inflammation in fat plays a crucial role in the development of obesity-related insulin resistance. *J Clin Invest* 112:1821–1830, 2003
28. Weisberg SP, McCann D, Desai M, Rosenbaum M, Leibel RL, Ferrante AW Jr: Obesity is associated with macrophage accumulation in adipose tissue. *J Clin Invest* 112:1796–1808, 2003
29. Takahashi S, Oida K, Ookubo M, Suzuki J, Kohno M, Murase T, Yamamoto T, Nakai T: Very low density lipoprotein receptor binds apolipoprotein E2/2 as well as apolipoprotein E3/3. *FEBS Lett* 386:197–200, 1996
30. Goudriaan JR, Tacken PJ, Dahlmans VE, Gijbels MJ, van Dijk KW, Havekes LM, Jong MC: Protection from obesity in mice lacking the VLDL receptor. *Arterioscler Thromb Vasc Biol* 21:1488–1493, 2001
31. Reaven GM: Banting lecture 1988: Role of insulin resistance in human disease. *Diabetes* 37:1595–1607, 1988
32. Considine RV, Sinha MK, Heiman ML, Kriauciunas A, Stephens TW, Nyce MR, Ohannesian JP, Marco CC, McKee LJ, Bauer TL, et al.: Serum immunoreactive-leptin concentrations in normal-weight and obese humans. *N Engl J Med* 334:292–295, 1996
33. Mahley RW, Nathan BP, Pitas RE: Apolipoprotein E: structure, function, and possible roles in Alzheimer's disease. *Ann N Y Acad Sci* 777:139–145, 1996
34. Masliah E, Mallory M, Ge N, Alford M, Veinbergs I, Roses AD: Neurodegeneration in the central nervous system of apoE-deficient mice. *Exp Neurol* 136:107–122, 1995
35. Chen Y, Lomnitski L, Michaelson DM, Shohami E: Motor and cognitive deficits in apolipoprotein E-deficient mice after closed head injury. *Neuroscience* 80:1255–1262, 1997
36. Bales KR, Verina T, Dodel RC, Du Y, Altstiel L, Bender M, Hyslop P, Johnstone EM, Little SP, Cummins DJ, Piccardo P, Ghetti B, Paul SM: Lack of apolipoprotein E dramatically reduces amyloid beta-peptide deposition. *Nat Genet* 17:263–264, 1997
37. Barger SW, Harmon AD: Microglial activation by Alzheimer amyloid precursor protein and modulation by apolipoprotein E. *Nature* 388:878–881, 1997
38. Trommsdorff M, Gotthardt M, Hiesberger T, Shelton J, Stockinger W, Nimpf J, Hammer RE, Richardson JA, Herz J: Reeler/disabled-like disruption of neuronal migration in knockout mice lacking the VLDL receptor and ApoE receptor 2. *Cell* 97:689–701, 1999
39. Zechner R, Moser R, Newman TC, Fried SK, Breslow JL: Apolipoprotein E gene expression in mouse 3T3–L1 adipocytes and human adipose tissue and its regulation by differentiation and lipid content. *J Biol Chem* 266:10583–10588, 1991

The structure of siglec-7 in complex with sialosides: leads for rational structure-based inhibitor design

Helen ATTRILL*†, Hirokazu TAKAZAWA†, Simone WITT‡, Soerge KELM‡, Rainer ISECKE§, Reinhard BROSSMER§, Takayuki ANDO¶, Hideharu ISHIDA¶, Makoto KISO¶, Paul R. CROCKER† and Daan M. F. van AALTEN*[1]

*Divisions of Biological Chemistry and Molecular Microbiology, School of Life Sciences, University of Dundee, Dundee DD1 5EH, Scotland, U.K., †Department of Cell Biology and Immunology, School of Life Sciences, University of Dundee, Dundee DD1 5EH, Scotland, U.K., ‡Centre for Biomolecular Interactions Bremen, Department of Biology and Chemistry, University Bremen, 28334 Bremen, Germany, §Biochemistry Center Heidelberg, University of Heidelberg, 69120, Heidelberg, Germany, and ¶Department of Applied Bioorganic Chemistry, Faculty of Applied Biological Sciences, Gifu University, 1-1 Yanagido, Gifu-shi, Gifu 501-1193, Japan

Siglecs (sialic acid binding Ig-like lectins) are transmembrane receptors for sialylated glycoconjugates that modulate cellular interactions and signalling events in the haematopoietic, immune and nervous systems. Siglec-7 is a structural prototype for the recently described family of immune inhibitory CD33-related siglecs and is predominantly expressed on natural killer cells and monocytes, as well as subsets of CD8 T-cells. Siglec-specific inhibitors are desired for the detection of masked and unmasked forms of siglecs, to aid in dissection of signalling pathways and as tools to investigate siglecs as potential therapeutic targets. As a first step towards this end, we present the crystal structure of siglec-7 in complex with a sialylated ligand, the ganglioside analogue DSLc4 [α(2,3)/α(2,6) disialyl lactotetraosyl 2-(trimethylsilyl)ethyl], which allows for a detailed description of the binding site, required for structure-guided inhibitor design. Mutagenesis and binding assays were used to demonstrate a key structural role for Lys^{131}, a residue that changes conformation upon sialic acid binding. Differences between the binding sites of siglec family members were then exploited using α-methyl Neu5Ac (*N*-acetylneuraminic acid) as a basic scaffold. A co-crystal of siglec-7 in complex with the sialoside inhibitor, oxamido-Neu5Ac [methyl α-9-(amino-oxalyl-amino)-9-deoxy-Neu5Ac] and inhibition data for the sialosides gives clear leads for future inhibitor design.

Key words: ganglioside, immune tyrosine-based inhibitory motif (ITIM), leucocyte, sialic acid, sialic acid binding Ig-like lectin (siglec), x-ray crystallography.

INTRODUCTION

The siglec (sialic acid binding Ig-like lectin) family is a group of transmembrane receptors with the ability to recognize sialic acids, a family of 9-carbon sugars which often cap the non-reducing ends of glycoconjugates in higher animals. Eleven siglecs have been described in humans, predominantly expressed on cells of the immune and haematopoietic systems [1,2]. Each siglec has a characteristic cell-type-dependent expression pattern and a distinct binding specificity for sialylated glycoconjugates [3]. Siglecs are often expressed in an overlapping manner on cells of the immune system and this may be important in allowing a given cell type the ability to respond to a spectrum of sialylated ligands.

With the exception of MAG [(myelin-associated glycoprotein)/siglec-4] and sialoadhesin (siglec-1), siglecs are thought to play a role in the suppression of immune cell activation [4], as they possess consensus ITIMs (immunoreceptor tyrosine-based inhibitory motifs) and ITIM-like motifs in their cytoplasmic tails. ITIMs have been described in a growing number of inhibitory receptors of the immune system [4a]. Their phosphorylation creates a high-affinity binding site for SH2 (Src-homology 2)-domain-containing phosphatases (SHP-1, SHP-2 and SHIP-1), and the subsequent antagonism of activating signals [5,6].

The human CD33-related siglecs (CD33 and siglec-5–siglec-11) and CD22 can interact with sialylated ligands presented on the same cell (*cis* interaction) [7], a phenomenon referred to as 'masking', as this prevents the binding of exogenously added ligands. For CD22 and some CD33-related siglecs expressed on blood leucocytes, B-cell activation results in partial unmasking [7,7a]. Cryptic sialic acid binding lectins on human blood leucocytes can be unmasked by sialidase treatment or cellular activation. However, for other siglecs such as siglec-7, which is expressed on NK (natural killer) cells, a variety of activation signals tested did not lead to unmasking [8]. The development of siglec-specific inhibitors based on a sialic acid template would provide useful tools for studying these receptors in their natural context. This has been achieved recently for CD22, by the modification of Neu5Ac (*N*-acetylneuraminic acid) at the C9 position with a biphenyl moiety, leading to a > 200-fold improvement in relative inhibitory potency compared with the unmodified sugar [9]. The utility of this inhibitor was clearly demonstrated when it was used to reveal that *cis* interactions are important in the inhibitory function of CD22 during B-cell activation [10].

Siglec-7 represents a good candidate for structure-based inhibitor design. It is the only CD33-related siglec for which the structure has been determined so far and therefore provides a template on which other members of this family may be modelled [11]. It displays a unique ligand binding preference, binding internally branched α(2,6)-linked sialic acid and α(2,8)-linked disialic acids [12]. Siglec-7 is expressed predominantly on NK

Abbreviations used: CHO, Chinese hamster ovary; DSLc4, α(2,3)/α(2,6) disialyl lactotetraosyl 2-(trimethylsilyl)ether; ESRF, European Synchrotron Radiation Facility; Gal, galactose; GalNAc, *N*-acetyl galactosamine; Glc, glucose; ITIM, immune tyrosine-based inhibitory motif; MAG, myelin-associated glycoprotein; Neu5Ac, *N*-acetylneuraminic acid; NK, natural killer cell; OPD, *O*-phenylenediamine; oxamido-Neu5Ac, methyl α-9-(amino-oxalyl-amino)-9-deoxy-Neu5Ac; PEG, poly(ethylene glycol); RBC, red blood cell; rmsd, root mean square deviation; siglec, sialic acid binding Ig-like lectin.

[1] To whom correspondence should be addressed (email dava@davapc1.bioch.dundee.ac.uk).

The co-ordinates and structural factors described in the present study have been deposited in the PDB (accession numbers 2DF3 and 2G5R).

cells and it has been shown to inhibit NK cell cytotoxicity towards target cells over-expressing the $\alpha(2,8)$-disialic acid-bearing ganglioside, GD3 [8]. The elevation of GD3 levels described for certain tumours (such as malignant melanoma and neuroblastoma) may, therefore, serve as an evasion strategy from NK killing [13]. A siglec-7-blocking compound could, therefore, have potential therapeutic value.

In the present study, we describe the first structural analysis of siglec-7 in complex with sialylated ligands: a ganglioside analogue, DSLc4 [$\alpha(2,3)/\alpha(2,6)$ disialyl lactotetraosyl 2-(trimethylsilyl)ethyl] [14], and a derivative of sialic acid, oxamido-Neu5Ac [methyl α-9-(amino-oxalyl-amino)-9-deoxyNeu5Ac]. In combination with binding assays, these structures give us an insight into what governs ligand binding and possible routes for rational inhibitor design.

MATERIALS AND METHODS

Expression and purification of siglec-7

The siglec-7 V-set domain was expressed and purified as described by Alphey et al. [11]. Briefly, the region encoding the siglec-7 V-set domain was cloned into the pDEF expression vector and transfected into CHO (Chinese hamster ovary) Lec1 cells [20]. A stable cell line was established using selection with hygromycin B. Cells were cultured in α-MEM (α-modified Eagle's medium) containing 5 % foetal calf serum and 1 % penicillin/streptomycin mix (Life Technologies). Siglec-7 was purified from the medium using an anti-siglec-7 polyclonal antibody affinity column followed by size-exclusion chromatography. The protein was concentrated to 6 mg/ml in 25 mM Tris (pH 8.0) and 75 mM NaCl.

Synthesis of oxamido-Neu5Ac

Oxamido-Neu5Ac was prepared from the methyl α-glycoside of 9-amino-9-deoxy-Neu5Ac by reaction with activated oxamic acid (R. Brossmer, unpublished work). The analogue was characterized by high-resolution nuclear magnetic resonance spectroscopy and fast atom bombardment MS.

Crystallization and data collection

For co-crystallization experiments, siglec-7 was incubated on ice for 10 min with a 20-fold molar excess of ligand (either DSLc4 or oxamido-Neu5Ac). Crystallization was conducted by using sitting-drop vapour diffusion, using 0.5 μl of reservoir solution added to a 0.5 μl drop of protein–ligand complex, and equilibrated with 100 μl of reservoir solution at 20 °C. The DSLc4–siglec-7 co-crystals used for data collection were grown in crystal screen CS CRYO condition forty-one {8.5 % iso-propanol, 0.095 M Hepes (pH 7.5), 17 % PEG [poly(ethylene glycol)]4000, 15 % glycerol}. A data set was collected to 1.90 Å (1 Å = 0.1 nm) at the ESRF (European Synchrotron Radiation Facility; Grenoble, France), beamline ID14 EH4 at 100 K using an ADSC Q4 CCD detector.

Co-crystals for siglec-7 and oxamido-Neu5Ac grew in a screen containing 30 % PEG 4000, 0.1 M sodium acetate (pH 4.6) and 0.2 M ammonium acetate. The crystal was cryogenically protected by soaking in the mother-liquor containing 10 % glycerol before freezing in a stream of nitrogen gas. A dataset was collected on ESRF beamline ID14 EH4 using an ADSC Q4 CCD detector at 100 K. Data were processed and scaled using the HKL suite of programs [21].

Structure determination and refinement

The structures for siglec-7–DSLc4 and siglec-7–oxamido-Neu5Ac were solved by molecular replacement using the program AMoRe [22] with the siglec-7 V-set domain structure (PDB code 1o7S [11]) as a search model. For both, a single solution was found with R-factors of 0.33 and 0.32 and correlation coefficients of 0.70 and 0.72 respectively. The model phases were used in WarpNTrace, which constructed 102 and 95 out of 127 residues respectively [23]. The models were refined using CNS (crystallography and NMR system) [24] software interspersed with manual model building in the program O [25]. Final refinement was performed using the program Refmac 5 [26].

After model building and the inclusion of water molecules in the refinement, the terminal sialic acid residue was placed into the unbiased $|F_o| - |F_c|, \Phi_{calc}$ electron density and further refinement was carried out. Strong connective $|F_o|$-$|F_c|, \Phi_{calc}$ electron density was observed across the 2-fold symmetry axis between the sialic acids of adjacent asymmetric units (Figure 1). The mode of binding which could best account for this density is that the ligand bridges two siglec molecules. Although the DSLc4 ligand is not symmetrical, it does possess a degree of pseudosymmetry in the tetrasaccharide unit NeuAcα(2,3)Galβ(1,3)GlcNAcβ-[NeuAcα(2,6)], the plane of pseudosymmetry being about the Galβ(1,3)GlcNAcβ bond. The electron density was interpreted to consist of the DSLc4 tetrasaccharide, as described above, spanning two siglec-7 monomers without preferential orientation. The density between the sialic acid residues is, therefore, made up of both Gal and GlcNAc, which occupy the same space at 50 % occupancy each. The tetrasaccharide was accommodated in the refinement by modelling it across the asymmetric unit at 50 % occupancy, which allows the symmetry operation to generate the ligand in the opposite orientation. Thus there is a 2-fold disorder combined with a 2-fold crystallographic axis. As these two orientations are mutually exclusive, the van der Waals interactions were turned off between these molecules. This satisfied the electron density between the binding sites. Electron densities for the other sugar residues were not observed. For the oxamido-Neu5Ac–siglec-7 complex, after the inclusion of water molecules and model building, oxamido-Neu5Ac was modelled into the unbiased $|F_o| - |F_c|, \Phi_{calc}$ density and was further refined.

Site-directed mutagenesis and expression of chimaeras

Mutagenesis was performed using the QuikChange site-directed mutagenesis kit (Stratagene) on a siglec-7–Fc chimaeric construct in a modified pEE14 plasmid. Successful mutagenesis was confirmed by sequencing. The plasmids were transiently transfected into COS-1 cells using FuGene 6 transfection reagent (Roche). The cells were cultured for a further 5 days in X-VIVO 10 serum-free medium (BioWhitaker) and the medium was harvested. The siglec-7–Fc concentration was assayed by ELISA and correct folding was confirmed by ELISA using anti-siglec-7 monoclonal antibodes (7.7a and 7.5a [27]).

RBC (red blood cell) binding assay

Siglec-7–Fc chimaeras were immobilized on microtitre plates to create a surface for human RBC capture [28]. For this procedure, a goat anti-(human Fc) antibody (Sigma) was coated on to immulon 4 HBX microtitre plates. The plates were washed with PBA (PBS, 0.1 % BSA and 10 mM sodium azide) and blocked with 5 % dried-milk powder. Serial dilutions of the siglec-7–Fc chimaera, 50 μl per well, were allowed to bind for 2 h at room temperature,

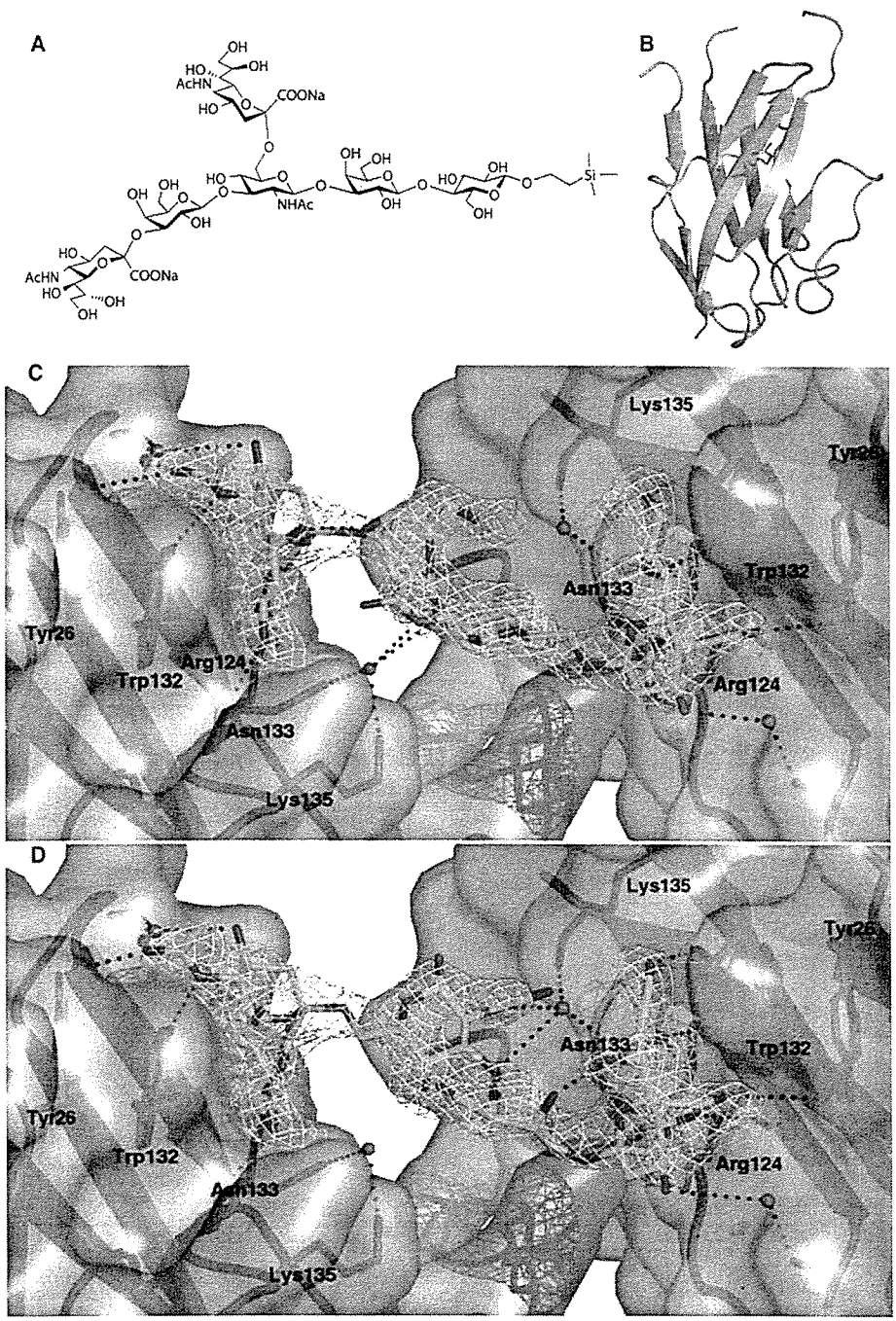

Figure 1 The siglec-7–DSLc4 interaction

(**A**) A schematic representation of the DSLc4 analogue. (**B**) The structure of the N-terminal, ligand-binding domain of siglec-7. β-strands are shown as blue arrows. The intrasheet disulphide bond is shown in green and the primary sialic acid binding Arg^{124} residue with carbons is in mauve. (**C** and **D**) show the DSLc4 ligand bridging two siglec-7 molecules related by a 2-fold crystallographic symmetry axis. Both orientations of the DSLc4 tetrasaccharide (green sticks) are shown modelled into an electron density that spans symmetry-related molecules. (**C**) The ligand is in the orientation: Neu5Acα(2,6)GlcNAcβ(3,1) Gal[Neu5Acα(2,3)], whereas in (**D**) the ligand is in the Neu5Acα(2,3)Galβ(1,3)GlcNAc[α(2,6)Neu5Ac] orientation. Unbiased (i.e. before inclusion of ligand) $|F_o|-|F_c|,\Phi_{calc}$ electron density contoured at 2.25 σ is shown as a yellow meshwork. The side-chains of residues that interact with the ligand are labelled, and water molecules bridging the protein and the ligand are shown as magenta spheres. The potential hydrogen-bonding network is shown as black dotted lines.

followed by three washes with PBA. A 100 μl aliquot of an RBC suspension was added to each well and allowed to bind for 30 min at room temperature. Unbound cells were removed by gentle washing and the cell layer was allowed to air-dry, followed by methanol fixation and permeabilization. The extent of RBC binding was assayed using OPD (*O*-phenylenediamine peroxidase) as the substrate [28] and by measuring A_{450} with a Cytofluor (PerSeptive Biosysytems) plate reader.

Hapten inhibition assays with sialic acid derivatives

For hapten inhibition assays, Fc chimaeras containing the three N-terminal domains of siglec-7 were purified in

Table 1 Data collection and refinement statistics

The co-ordinates and structure factors have been deposited with the PDB (entries 2DF3 and 2G5R). Statistical analysis results for the highest resolution shell are shown in parentheses.

Data Collection	Siglec-7–DSLc4	Siglec-7–oxamido-Neu5Ac
Wavelength (Å)	0.933	0.933
Resolution (Å)	25–1.90 (1.97–1.90)	25–1.60 (1.66–1.60)
Space group	$P4_12_12$	$P4_12_12$
Unit cell (Å)	a = b = 53.07, c = 92.88	a = b = 52.93, c = 93.24
Reflections:		
Observed	46855	74536
Unique	11014	17748
Redundancy	4.3 (3.8)	4.2 (2.2)
R_{merge}	0.078 (0.445)	0.043 (0.338)
$I/\sigma I$	15.5 (3.1)	21.5 (2.0)
Completeness (%)	99.3 (94.0)	97.5 (78.9)
R_{free} reflections	523	893
R_{cryst} (%)	19.7	21.4
R_{free} (%)	23.7	22.8
Total number of atoms	1119	1053
Protein	944	904
Water	95	102
Glycan	14	14
Ligand	66	27
Protein (Å^2)	20	18
Water (Å^2)	27	27
Glycan (Å^2)	33	27
Ligand (Å^2)	24	44
rmsd from ideal geometry		
Bond lengths (Å)	0.014	0.015
Bond angles (°)	1.65	1.35
Main chain B (Å^2)	1.55	1.77

Table 2 Hydrogen-bond network

Potential hydrogen-bonds and the distances between atoms are indicated.

Ligand–protein hydrogen-bonds

DSLc4 atom	Protein atom	Distance (Å)
Neu5Ac (α2,6)		
O1A	Arg^{124} NH2	3.0
O1B	Arg^{124} NH1	2.8
N5	Lys^{131} CO	2.7
O5	Tyr^{26} OH	3.4
O8	Asn^{133} N	2.9
O9	Lys^{135} NZ	2.8
O9	Asn^{133} CO	2.8
Neu5Ac (α2,3)		
O1A	Arg^{124} NH2	2.7
O1B	Arg^{124} NH1	2.9
N5	Lys^{131} CO	3.3
O5	Tyr^{26} OH	4.3
O8	Asn^{133} N	3.0
O9	Lys^{135} NZ	3.1
O9	Asn^{133} CO	3.1

DSLc4–protein hydrogen-bonds mediated by water

Atom	Water molecule	Distance (Å)
Gal (α2,3) O3	105	3.4
GlcNAc (α2,3) N2	105	3.4
Asn^{133} ND2	105	2.6
Lys^{135} NZ	105	2.7
O4 Neu5Ac (α2,6)	110	3.1
O4 Neu5Ac (α 2,3)	110	3.8
Asn^{129} CO	110	2.6

Intramolecular hydrogen-bonds

DSLc4 atom	DSLc4 atom	Distance (Å)
Neu5Ac (α2,3) O7	Gal O4	2.7
Neu5Ac O8 (α2,6)	Neu5Ac O9	2.8
Neu5Ac O8 (α2,3)	Neu5Ac O9	3.4

Protein A–agarose from tissue culture supernatants of stably transfected CHO cells, as described by Yamaji et al. [12]. Microtitre plates with covalently linked Neu5Ac (GlycoWells from Lundonia, Lund, Sweden) were used as a binding target. Prior to the binding assay, the Fc-chimaeras (final concentration 200 ng/ml) were complexed with an anti-Fc antibody coupled to alkaline phosphatase (1:1000 dilution, supplied by Dianova, Hamburg, Germany) in HBS-T [10 mM Hepes, 150 mM NaCl (pH 7.4) and 0.05 % Tween 20] for 15–30 min at room temperature. A 30 μl aliquot of this pre-complex was added per well and incubated for 4 h at 4 °C in the presence or absence of sialic acid derivatives. After five washes with HBS-T, the amount of bound alkaline phosphatase was quantified by determination of the initial reaction velocity using fluorescein disphosphate (15 μM) as substrate. To determine the concentration required for 50 % inhibition (IC_{50}), the inhibitor was used at seven different concentrations spanning two orders of magnitude. Each concentration experiment was carried out in triplicate and assays were repeated at least three times.

RESULTS AND DISCUSSION

The DSLc4 complex

Sparse matrix-sampling screening for siglec-7 co-crystallization with the DSLc4 ganglioside analogue (Figure 1A) yielded an unusually high number of hits: over 20 out of 144 conditions within a period of two days. All crystals were of a bi-pyramidal morphology, with a very similar appearance to that of an uncomplexed crystal form of siglec-7. Synchrotron diffraction data were collected to a resolution of 1.90 Å (Table 1). The unit cell dimensions were also similar to apo-siglec-7 and indexed in the same space group, $P4_12_12$. Interpretation of the ligand density revealed that an ordered tetrasaccharide unit [Neu5Acα(2,3)Galβ(1,3)GlcNAc[α(2,6)Neu5Ac] bridged the binding sites of siglec-7 in adjacent asymmetric units across a crystallographic 2-fold axis of rotation, with 2-fold disorder (Figures 1C and 1D). The net result is the stabilization of the same crystal packing structure, as observed for native siglec-7, and perhaps explains the unusual promotion of crystal formation. Comparison of the native and complexed form [rmsd (root mean square deviation) = 0.73 Å on all C_α atoms] revealed that there is little deformation in crystal packing with only a 0.9 Å decrease in the c-axis of the unit cell.

Within the ligand, intramolecular hydrogen-bonding between the Gal C4 hydroxy group and the Neu5Ac [α(2,3) linkage] C7 hydroxy group stabilizes the tetrasaccharide (Table 2), tethering it between the two symmetry-related siglec-7 molecules (Figures 1C and 1D). Although no direct contacts are made with the protein molecules beyond the terminal sugars, water-mediated hydrogen bonds are made between Asn^{133} and Lys^{135}, and the C3 nitrogen of the GlcNAc and the oxygen of the glycosidic bond between Gal and GlcNAc [in the α(2,3) linkage orientation] (Figure 1D and Table 2).

It is not clear whether the contacts observed outside the primary sialic acid binding site in this crystal structure represent 'natural' or artificial contacts which arise from crystal packing. Binding studies have shown that both the sialic acid linkage and the adjacent sub-terminal sugar are key contributors to siglec ligand specificity. Siglec-7 displays only a weak interaction with ligands bearing α(2,3)-linked sialic acids [12]. Comparison of the binding of siglec-7 with branched α(2,3)/α(2,6) disialyl ligands, such as

Table 3 Glycosidic bond angles

Dihedral angles for the glycosidic bonds of DSLc4 and equivalent linkages in structures deposited in the PDB were analysed using the Carbohydrate Ramachandran Plot (CARP) tool of the Carbohydrate Structure Suite (CSS) [29] (http://www.dkfz.de/spec/css/index.php). The dihedral angles for the Galβ(1,3)GlcNAc-linkage are defined as: Φ = O5-C1-O3′-C3′ and ψ = C1-O3′-C3′-C4′. For the Neu5Acα(2,3)Gal linkage: Φ = C1-C2-O3′-C3′ and ψ = C2-O2-C3′-C4′. For the Neu5Acα(2,6)GlcNAc linkage: Φ = C1-C2-O6′-C6′, ψ = C2-O2-C6′-C5′. The stereochemical conformation is given after the torsion angle, and is defined as: 0 to 30 synperiplanar (*sp*); 30° to 90° and -30° to -90° synclinal (*sc*); 90° to 150° and -90° to -150° anticlinal (*ac*); and ±150° to 180° antiperiplanar (*ap*). No., number of ligand examples in the PDB.

	DSLc4		Survey of PDB		
Linkage	Φ	ψ	Φ	ψ	No.
Neu5Acα(2,6)GlcNAc	−84 (*ac*)	−169 (*ap*)	−85 to −82 (*sc*), +22 to +27 (*sp*)	+190 to +144 (*ap*)	5
Galβ(1,3)GlcNAc	−41 (*sc*)	−59 (*sc*)	+28 to +63 (*sc*)	−27 to +25 (*sp*)	12
Neu5Acα(2,3)Gal	−133 (*ac*)	−42 (*sc*)	−35 to −75 (sc), +175 to +190 (*ap*)	+26 to −44 (*sp*, *sc*)	62

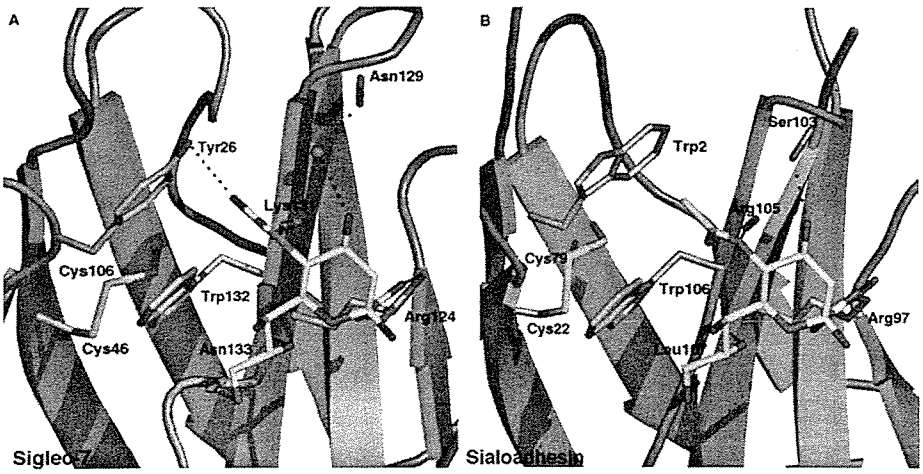

Figure 2 Comparison of sialic-acid-binding by siglec-7 (A) with sialoadhesin (B)

An intra-sheet disulphide bond (green sticks) results in the widening of the β sandwich, exposing hydrophobic residues that contribute to the primary sialic acid binding site. In both structures the sialic acid carboxylate is anchored by an interaction with a conserved arginine residue. In siglec-7 the replacement of tryptophan (Trp^2) with tyrosine (Tyr^{26}), results in rotation of the C5 N-acetyl group to allow hydrogen-bonding with the side-chain hydroxy group.

disialylgalactosyl-globoside and disialyl Lewis^a motifs and their monosialylated, α(2,3) sialic-acid-bearing equivalents, shows that it is the α(2,6) branch that is required for higher affinity binding [15,16]. Therefore we would expect to observe selective binding of the α(2,6) branch, rather than equal binding, as in this crystal structure. Furthermore, the C-C′ loop, which has been implicated in directing ligand binding specificity, is disordered in the siglec-7–DSLc4 complex. There are two possible explanations for the absence of direct contacts between side-chain and subterminal sugars in this crystal structure. First, regions of siglec-7, such as the C-C′ loop, may adopt different conformations in order to interact with the different linkages, and 2-fold disorder in the ligand may make such flexible protein interactions difficult to see in the electron density maps. Second, the interaction of the capping sialic acids drives cross-linking and stabilization of crystal packing, and the ligand is held in an artificial manner. Nevertheless, the water-mediated interaction between the ligand and residues Asn^{133} and Lys^{135}, suggests that they may play a genuine role in ligand binding.

The ligand bridges two binding sites that are relatively close together, which possibly results in conformational strain in the ligand. This can be examined by comparing the dihedral bond angles of the DSLc4 ligand with those of the same linkages in other previously determined glycan structures. The ψ and Φ angles of Neu5Acα(2,3)Gal and Neu5Acα(2,6)GlcNAc linkages lie within regions common to other glycans deposited in the PDB (Table 3). The distortion lies in the Galβ(1,3)GlcNAc linkage. In structures deposited in the PDB, all ψ angles fall within the synclinal conformation, +28 to +68. In DSLc4 this lies in the opposite orientation at −41°. The Φ angle of this bond is again different, −59° (synclinal), compared with a synperiplanar conformation (−27 to +25°) adopted by other structures. The net result is that the ring-faces of Gal and GlcNAc in the DSLc4 glycan bound to siglec-7 lie at a 90° angle relative to each other, whereas in the other structures the rings are co-planar. The straining of the ligand is also reflected in the contacts made by each Neu5Ac group and, overall, the α(2,6)-linked Neu5Ac is more intimately associated with the binding site (Table 2).

Sialic acid binding by siglec-7

Siglec-7 makes several contacts with the DSLc4 terminal sialic acid that are similar to those observed in the crystal structure of sialoadhesin in complex with 3′ sialyllactose (Figure 2). Arg^{124} forms a salt-bridge with the sialic acid carboxylate, an interaction that is essential for sialic acid binding in all siglecs [17,18] (Figure 2A). Hydrogen-bonds between the glycerol hydroxy groups at the C8 and C9 positions, and the nitrogen and protein backbone of the C5 *N*-acetyl group are conserved [19]. In both structures a tryptophan residue makes hydrophobic contacts with the glycerol moiety of the sialic acid. Sialoadhesin makes additional contacts with the primary sialic acid via a hydrogen-bond between the C4 hydroxy group and the carbonyl backbone of Ser^{103}, and hydrophobic interactions between the *N*-acetyl methyl

and Trp[2] (Figure 2B). In the siglec-7–DSLc4 structure these contacts differ. An amino acid insertion in the F–G loop of sialoadhesin projects it towards the binding site, bringing the carbonyl oxygen of Ser[103] to within hydrogen-bonding distance of the C4 hydroxy group. In siglec-7, the equivalent residue (Asn[129]), is 4.7 Å distant from the C4 hydroxy group. Instead, this interaction is replaced by a water-mediated hydrogen-bond. The tryptophan residue, which interacts with the *N*-acetyl methyl in sialoadhesin, is replaced with a tyrosine (Tyr[26]) residue in siglec-7. In the siglec-7–DSLc4 complex the orientation of the acetyl group is rotated 180°, which allows the oxygen to form a weak hydrogen-bond with the tyrosine hydroxy group.

Flexibility within the binding site

Comparison of the apo structures (PDB accession numbers, 1o7S and 1NKO; 1o7V is excluded from this analysis as a loop from a symmetry related molecule occupies the binding site) of siglec-7 with that of the complexed form revealed that there is little overall positional change in the residues that form the binding site (rmsd = 1.2 Å on all atoms, Figure 3A). One notable difference is that in the apo structures the side-chain of Lys[131] obscures access to the guanidinium group of Arg[124]. In the complexed form this residue moves away to reveal the primary arginine residue, which allows it to interact with the carboxy group of sialic acid (Figure 3A). A similar phenomenon is observed when comparing the apo (PDB accession number 1QFP) and bound (PDB accession number 1QFO) forms of sialoadhesin, in which the 'essential' arginine residue, Arg[97], is masked by the side-chain of Arg[105] (Figure 3B). Upon ligand-binding, Arg[105] moves away (by 3.8 Å), and Arg[97], no longer blocked by Arg[105], moves 1.8 Å into a position where it can engage the carboxylate of sialic acid. With the exception of siglec-4/MAG, in all the human siglecs the residue equivalent to Lys[131] in siglec-7 is either an arginine or a lysine residue (in siglec-4/MAG it is glutamine). When Lys[131] was replaced with alanine by site-directed mutagenesis, this, unexpectedly, abolished binding of siglec-7–Fc to RBCs (Figure 3C), an effect comparable with that seen when the essential Arg[124] was replaced with alanine (Figure 3C). Both mutant proteins appeared to be correctly folded as judged by their normal reactivity with anti-siglec-7 monoclonal antibodies (results not shown). These results suggest that rather than masking Arg[124] from ligands, Lys[131] is essential for ligand engagement. What biological significance this has is unclear; for example this residue may protect the primary arginine residue from non-productive or low-affinity interactions with organic or non-organic anions, which could disrupt binding-site integrity.

Sialic-acid-based inhibitor design

Siglec-7 interacts only weakly with a Neu5Ac moiety. This has also been observed in hapten inhibition assays (Table 4) in which 3 mM methyl-α-Neu5Ac leads to only 35 % inhibition. However, hydroxylation of the *N*-acetyl group to *N*-glycolyl enhances binding, since the inhibitory acitivity of methyl-α-Neu5Gc (methyl-α-5-glycolylneuraminic acid) is increased at least 2-fold. By contrast, this sialic acid is not bound by sialoadhesin or siglec-4/MAG (Kelm et al. [28]). Molecular modelling (results not shown) suggests that this additional hydroxy group could lie within hydrogen-bonding distance (between 2.7–2.6 Å) of the side-chain of Tyr[26]. For sialoadhesin or siglec-4, in which this position is occupied by a tryptophan residue, such a modification may be sterically unfavourable.

In hapten inhibition assays, Neu5Ac derivatized with an oxamido group at C9 of the glycerol side-chain (Figure 4B), was found to have at least 3-fold greater inhibitory activity than Neu5Ac (Table 4). By contrast, this sialic acid derivative inhibited sialoadhesin approx. 5-fold less compared with Neu5Ac (results

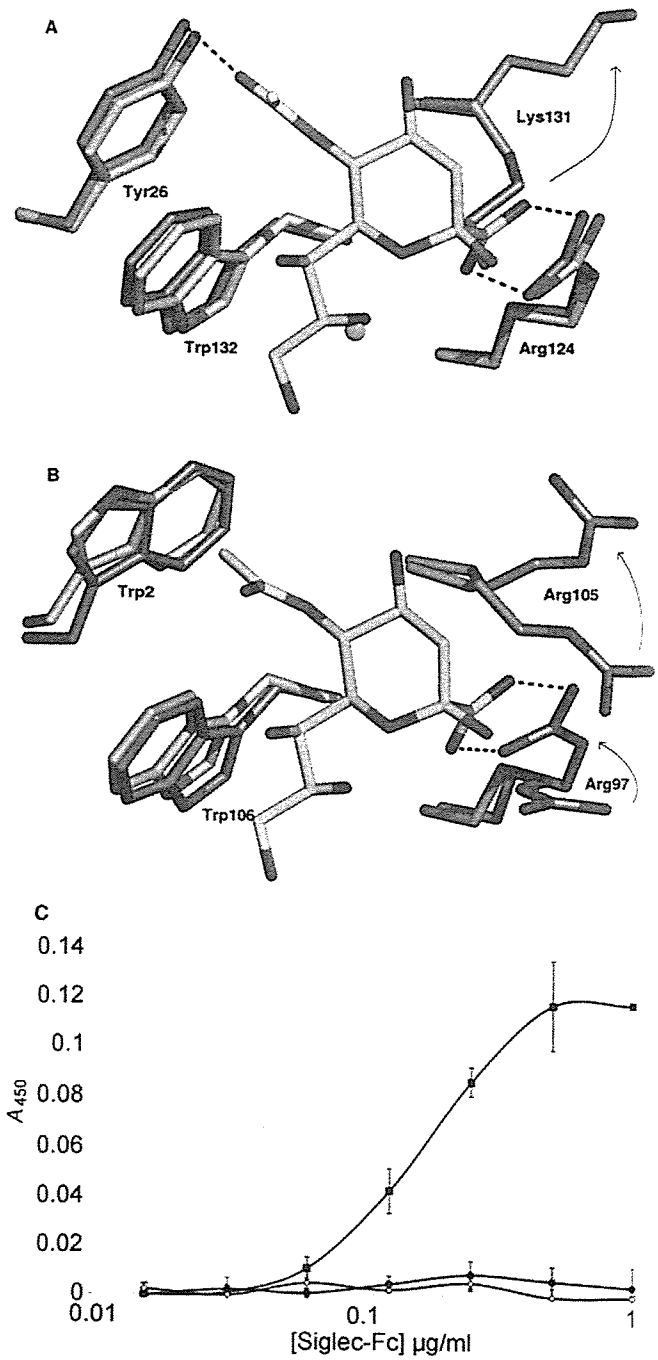

Figure 3 The role of Lys[131]

The binding of sialic acid is accompanied by small, conserved conformational changes. Superposition of the apo and ligand-bound crystal structures of siglec-7 (**A**) and sialoadhesin (**B**), show that there is a conserved movement upon ligand binding. Side-chains which remain static are shown in cream (apo) and grey (bound ligand), whereas those that move are shown with orange (apo) and pink (ligand-bound) carbons. Arrows indicate the conformational change that accompanies ligand binding. A water molecule (green sphere), which hydrogen-bonds with the backbone nitrogen of Asn[133] of siglec-7 is displaced by the sialic acid C8 hydroxy group. (**C**) An RBC-binding assay was used as a measure of sialic acid-dependent binding. Serial dilutions of siglec-7–Fc chimaeras, wild-type (■), and mutants R124A (◇) and K131A (●), were immobilized on microtitre plates and the extent of RBC binding was measured by an OPD assay.

Table 4 Hapten inhibition assay data

Sialic acid derivative	IC_{50} (μM)
Me-α-Neu5Ac	>3000 (35%)
Me-α-oxamido-Neu5Ac	1600
Me-α-5-N-glycolyl-Neu	2000

not shown). To examine this differential binding, siglec-7 was co-crystallized with a 20-fold molar excess of oxamido-Neu5Ac, synchrotron diffraction data were collected to 1.6 Å, the structure was solved by molecular replacement and refined (rmsd = 0.83 Å on all C_α atoms compared with the apo structure, Table 4). The structure of the siglec-7–oxamido-Neu5Ac complex revealed that many of the important contacts are maintained: salt-bridge formation between the carboxylate and Arg^{124}, hydrogen-bonding between the Asn^{133} carbonyl and the C5 *N*-acetyl group, hydrophobic interactions between the derivatized glycerol chain and Trp^{132}, and hydrogen-bonding between the C8 hydroxy group and the backbone nitrogen of Asn^{133} (Figure 4A). The hydrogen-bond formed between the C9 hydroxy group of sialic acid and the Asn^{133} carbonyl is directly replaced by the nitrogen of the oxamido group. An additional hydrogen-bond is formed between C11 oxygen and the backbone nitrogen of Lys^{131}. Superposition of oxamido-Neu5Ac with sialoadhesin structures suggests that the weaker binding of this compound could be due to a steric clash of the side-chain of Val^{109} with the terminal amide of the oxamido group (Figure 4D).

Derivatization of Neu5Ac at the C9 position by hydrophobic moieties has yielded increased binding to other siglecs, namely human and murine CD22 and CD33, and sialoadhesin [9,10]. Crystal structures of sialoadhesin in complex with sialiosides demonstrated that this was predominantly due to the presence of a 'hydrophobic gate' formed by Val^{109} and Leu^{107} [9], which sandwiches the hydrophobic substituents. By sequence alignment and modelling of members of the siglec family, Zaccai et al. [9] proposed that variations in the residues which create this cleft

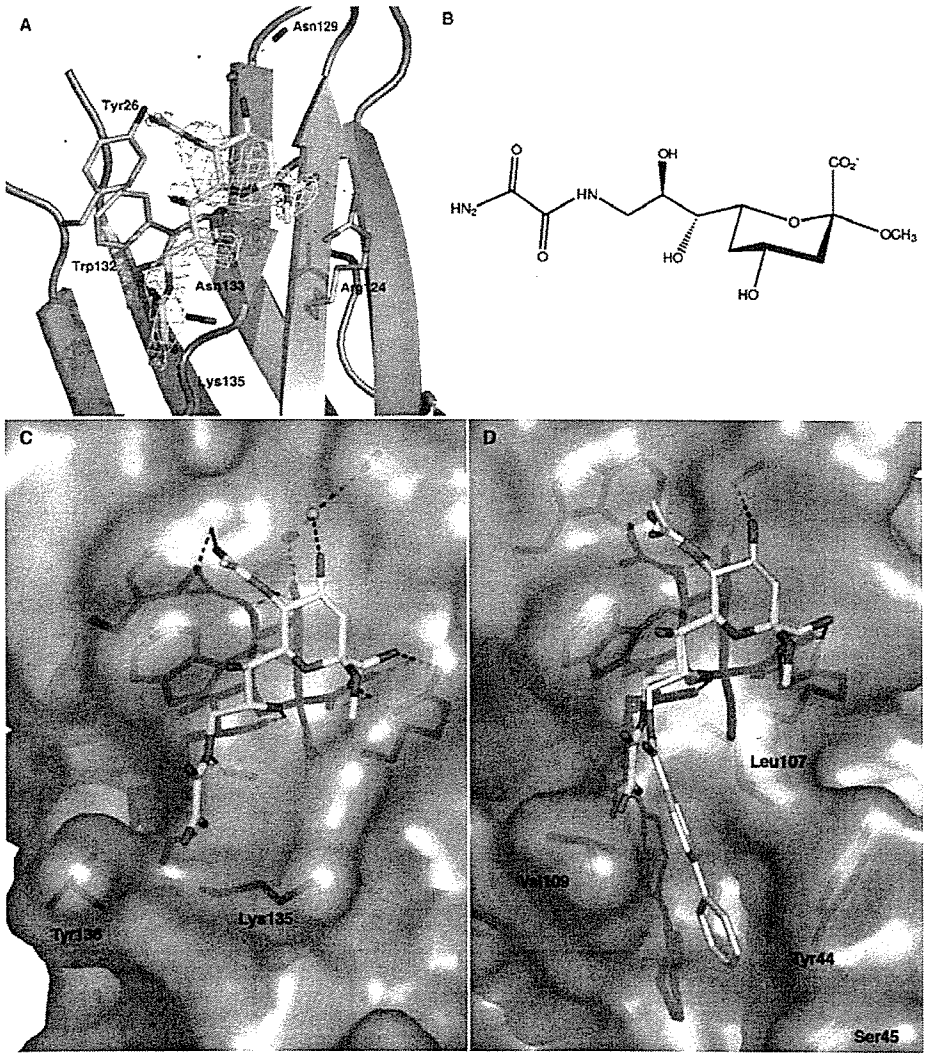

Figure 4 Binding of oxamido-Neu5Ac by siglec-7

Siglec-7 is shown in complex with oxamido-Neu5Ac (**A**) with unbiased $|F_o|-|F_c|,\Phi_{calc}$ density contoured at 2.25 σ. The methyl-α-glycoside of 9-amino-9-deoxy-Neu5Ac was derivatized with an oxamido group at the C9 position (**B**). A surface representation of siglec-7 (**C**) and sialoadhesin (**D**) shows that both possess a hydrophobic gate, formed by Lys^{135} and Tyr^{136}, and Leu^{107} and Val^{109} respectively. However, these channels lie at divergent angles. (**D**) The sialoadhesin9–BIP(biphenyl)-Neu5Ac complex (BIP is shown with cream carbon atoms) is shown in order to highlight the orientation of the hydrophobic gate. Additionally, residues which participate in BIP binding are indicated. Superimposition of oxamido-Neu5Ac (cyan carbons) on to sialoadhesin (**D**), shows that Val^{109} could sterically hinder binding.

(which are not well conserved) might contribute to the differences in binding affinity. In siglec-7 the walls of this hydrophobic groove are formed by Lys^{135} and Tyr^{136} (Figure 4C), and differs significantly from that of sialoadhesin (Figure 4D). The hydrophobic gate of siglec-7 is deeper, with much steeper sides, and the axis of the cleft is skewed by approx. 45° compared with that of sialoadhesin.

Such differences provide promising leads for the design of siglec-specific sialosides: of the human siglecs, siglec-7 is unique in having tryptophan and lysine residues forming the hydrophobic gate. In the siglec-7–oxamido-Neu5Ac structure, the oxamido group is anchored by a hydrogen-bond with its terminal amide, aligning it with the axis of the channel. Therefore the addition of aromatic moieties to the C11 nitrogen of oxamido-Neu5Ac may enhance binding and specificity. This could be complemented by the use of Neu5Gc as the template for derivatization.

Conclusions

In the present study, we have described the structure of siglec-7 in complex with a ganglioside analogue of DSLc4. This structure has allowed detailed analysis of the primary sialic acid binding site of siglec-7. Furthermore, a sialic acid analogue carrying an oxamido group at C9 was studied in complex with siglec-7. On the basis of this structure, the 3–4-fold increase in relative inhibitory potency when compared with methyl-α-Neu5Ac has been explained in molecular detail. This compound will serve as a guide for further substitutions, with the aim of creating a ligand of high affinity and high selectivity towards siglec-7.

This work was supported by BBSRC grant B14010 awarded to P.R.C., and D.M.F.vA. S.K. and S.W. were supported by Deutsche Forschungsgemeinschaft (grant DFG Ke428.3-3). D.M.F.vA. is supported by a Wellcome Trust Senior Research Fellowship.

REFERENCES

1 Crocker, P. R. and Varki, A. (2001) Siglecs in the immune system. Immunology **103**, 137–145
2 Crocker, P. R. (2005) Siglecs in innate immunity. Curr. Opin. Pharmacol. **4**, 431–437
3 Crocker, P. R. (2002) Siglecs: sialic-acid-binding immunoglobulin-like lectins in cell-cell interactions and signalling. Curr. Opin. Struct. Biol. **12**, 609–615
4 Crocker, P. R. and Varki, A. (2001) Siglecs, sialic acids and innate immunity. Trends Immunol. **22**, 337–342
4a Staub, E., Rosenthal, A. and Hinzmann, B. (2004) Systematic identification of immunoreceptor tyrosine-based inhibitory motifs in the human proteome. Cell Signal. **4**, 435–456
5 Yusa, S. and Campbell, K. S. (2003) Src homology region 2-containing protein tyrosine phosphatase-2 (SHP-2) can play a direct role in the inhibitory function of killer cell Ig-like receptors in human NK cells. J. Immunol. **170**, 4539–4547
6 Connolly, N. P., Jones, M. and Watt, S. M. (2002) Human siglec-5: tissue distribution, novel isoforms and domain specificities for sialic acid-dependent ligand interactions. Br. J. Haematol. **119**, 221–238
7 Razi, N. and Varki, A. (1998) Masking and unmasking of the sialic acid-binding lectin activity of CD22 (Siglec-2) on B lymphocytes. Proc. Natl. Acad. Sci. U.S.A. **95**, 7469–7474
7a Razi, N. and Varki, A. (1999) Cryptic sialic acid binding lectins on human blood leukocytes can be unmasked by sialidase treatment or cellular activation. Glycobiology **11**, 1225–1234
8 Nicoll, G., Arvil, T., Lock, K., Furukawa, K., Bovin, N. and Crocker, P. R. (2003) Ganglioside GD3 expression on target cells can modulate NK cell cytotoxicity via siglec-7-dependent and independent mechanisms. Eur. J. Immunol. **33**, 1642–1648
9 Zaccai, N. R., Maenaka, K., Maenaka, T., Crocker, P. R., Brossmer, R., Kelm, S. and Jones, E. Y. (2003) Structure-guided design of sialic acid-based siglec inhibitors and crystallographic analysis in complex with sialoadhesin. Structure **11**, 557–567
10 Kelm, S., Gerlach, J., Brossmer, R., Danzer, C. P. and Nitschke, L. (2002) The ligand-binding domain of CD22 is needed for inhibition of the B cell receptor signal, as demonstrated by a novel human CD22-specific inhibitor compound. J. Exp. Med. **195**, 1207–1213
11 Alphey, M. S., Attrill, H., Crocker, P. R. and van Aalten, D. M. F. (2003) High resolution crystal structures of siglec-7. Insights into ligand specificity in the Siglec family. J. Biol. Chem. **278**, 3372–3377
12 Yamaji, T., Teranishi, T., Alphey, M. S., Crocker, P. R. and Hashimoto, Y. (2002) A small region of the natural killer cell receptor, Siglec-7, is responsible for its preferred binding to α 2,8-disialyl and branched α 2,6-sialyl residues. A comparison with siglec-9. J. Biol. Chem. **277**, 6324–6332
13 Soulieres, D., Rousseau, A., Deschenes, J., Tremblay, M., Tardif, M. and Pelletier, G. (1991) Characterization of gangliosides in human uveal melanoma cells. Int. J.Cancer **49**, 498–503
14 Ando, T., Ishida, H. and Kiso, M. (2003) First total synthesis of α-(2–>3)/α-(2–>6)-disialyl lactotetraosyl ceramide and disialyl Lewis A ganglioside as cancer-associated carbohydrate antigens. Carbohydr. Res. **38**, 503–514
15 Ito, A., Handa, K., Withers, D. A., Satoh, M. and Hakomori, S. (2001) Binding specificity of siglec7 to disialogangliosides of renal cell carcinoma: possible role of disialogangliosides in tumor progression. FEBS Lett. **504**, 82–86
16 Miyazaki, K., Ohmori, K., Izawa, M., Koike, T., Kumamoto, K., Furukawa, K., Ando, T., Kiso, M., Yamaji, T., Hashimoto, Y. et al. (2004) Loss of disialyl Lewis(a), the ligand for lymphocyte inhibitory receptor sialic acid-binding immunoglobulin-like lectin-7 (siglec-7) associated with increased sialyl Lewis(a) expression on human colon cancers. Cancer Res. **64**, 4498–4505
17 Angata, T. and Varki, A. (2000) Siglec-7: a sialic acid-binding lectin of the immunoglobulin superfamily. Glycobiology **10**, 431–438
18 Crocker, P. R., Vinson, M., Kelm, S. and Drickamer, K. (1999) Molecular analysis of sialoside binding to sialoadhesin by NMR and site-directed mutagenesis. Biochem. J. **341**, 355–361
19 May, A. P., Robinson, R. C., Vinson, M., Crocker, P. R. and Jones, E. Y. (1998) Crystal structure of the N-terminal domain of sialoadhesin in complex with 3′ sialyllactose at 1.85 Å resolution. Mol. Cell. **1**, 719–728
20 Stanley, P. and Chaney, W. (1985) Control of carbohydrate processing: the lec1A CHO mutation results in partial loss of N-acetylglucosaminyltransferase I activity. Mol. Cell Biol. **5**, 1204–1211
21 Otwinowski, Z. and Minor, W. (1997) Processing of X-ray diffraction data collected in oscillation mode. Methods Enzymol. **276**, 307–326
22 Navaza, J. (1994) AMoRe: an automated package for molecular replacement. Acta Crystallogr. Sect. A Found. Crystallogr. **50**, 157–163
23 Perrakis, A., Morris, R. and Lamzin, V. S. (1999) Automated protein model building combined with iterative structure refinement. Nat. Struct. Biol. **6**, 458–463
24 Brunger, A. T., Adams, P. D., Clore, G. M., DeLano, W. L., Gros, P., Grosse-Kunstleve, R. W., Jiang, J. S., Kuszewski, J., Nilges, M., Pannu, N. S. et al. (1998) Crystallography and NMR system: a new software system for macromolecular structure determination. Acta Crystallogr. Sect. D Biol. Crystallogr. **54**, 905–921
25 Jones, T. A., Zou, J. Y., Cowan, S. W. and Kjeldgaard (1991) Improved methods for building protein models in electron density maps and the location of errors in these models. Acta Crystallogr. Sect. A Found. Crystallogr. **47**, 110–119
26 Murshudov, G. N., Vagin, A. A. and Dodson, E. J. (1997) Refinement of macromolecular structures by the maximum-likelihood method. Acta Crystallogr. Sect. D Biol. Crystallogr. **53**, 240–255
27 Nicoll, G., Ni, J., Liu, D., Klenerman, P., Munday, J., Dubock, S., Mattei, M. G. and Crocker, P. R. (1999) Identification and characterization of a novel siglec, siglec-7, expressed by human natural killer cells and monocytes. J. Biol. Chem. **274**, 34089–34095
28 Kelm, S., Pelz, A., Schauer, R., Filbin, M. T., Tang, S., de Bellard, M. E., Schnaar, R. L., Mahoney, J. A., Hartnell, A., Bradfield, P. et al. (1994) Sialoadhesin, myelin-associated glycoprotein and CD22 define a new family of sialic acid-dependent adhesion molecules of the immunoglobulin superfamily. Curr. Biol. **4**, 965–972
29 Lutteke, T., Frank, M. and von der Lieth, C. W. (2005) Carbohydrate structure suite (CSS): analysis of carbohydrate 3D structures derived from the PDB. Nucleic Acids Res. **33**, 242–246

Received 16 January 2006/15 March 2006; accepted 20 April 2006
Published as BJ Immediate Publication 20 April 2006, doi:10.1042/BJ20060103

Available online at www.sciencedirect.com
SCIENCE DIRECT®
Carbohydrate Research 341 (2006) 1522–1532
Carbohydrate RESEARCH

Studies on the α-(1→4)- and α-(1→8)-fucosylation of sialic acid for the total assembly of the glycan portions of complex HPG-series gangliosides ☆

Hiromune Ando,[a,*] Hiroyo Shimizu,[b,c] Yukari Katano,[b,c] Yusuke Koike,[b,c] Sachiko Koizumi,[b,c] Hideharu Ishida[b,c] and Makoto Kiso[b,c,*]

[a] *Division of Instrumental Analysis, Life Science Research Center, Gifu University, 1-1 Yanagido, Gifu-shi, Gifu 501-1193, Japan*
[b] *Department of Applied Bioorganic Chemistry, Faculty of Applied Biological Sciences, Gifu University, 1-1 Yanagido, Gifu-shi, Gifu 501-1193, Japan*
[c] *CREST, Japan Science and Technology Corporation (JST), 1-1 Yanagido, Gifu 501-1193, Japan*

Received 7 February 2006; received in revised form 7 March 2006; accepted 13 March 2006
Available online 5 April 2006

Abstract—A synthetic study on α-(1→4) and α-(1→8)-fucosylation of sialic acid is reported, with the ultimate aim being the total assembly of the glycan portion of HPG-series gangliosides. In both types of fucosylations, the combination of a phenylthio fucosyl donor and a 1,5-lactamized acceptor provided high-yielding glycosylations to afford α-fucosyl-sialic acid sequences. The obtained α-Fuc*p*-(1→8)-Neu*p*NAc glycan having a 1,5-lactam bridge has been successfully transformed into the corresponding glycosyl donor.

Keywords: Fucosylation; 1,5-Lactamized sialyl acceptor; Ganglioside HPG-1; Ganglioside HPG-7

1. Introduction

The broad diversity of sialic acid structures has been demonstrated by numerous studies in the field of natural product chemistry.[1] For example, N-glycosylation, de-N-acetylation, O-methylation, O-sulfonylation, and O-acetylation are representative modifications of sialic acids. In addition to these structural modifications, sialic acid often condenses with other sialic acid residues, forming homo-oligomers and polymers. Presumably, the structural polymorphism of sialic acid relates to the complex biological functions of sialo-oligosaccharides in cells.

To clarify the molecular basis underlying the biological roles of these various structural motifs, we have engaged in a long-term project on the synthesis of sialoglycoconjugates. In particular, our recent focus has turned to the synthesis of oligosaccharides containing intricate sialic acid congeners. We thus have previously reported the synthesis of 1,5-lactamized-[2] and 5-amino[3]-sialyl Lewis X homologues, and very recently, the first synthesis of the glycan portions of HLG-2 and Hp-s6 gangliosides,[4] which have partially modified disialic acid residues in their glycan skeletons. In the latest synthesis, we developed highly reactive 1,5-lactamized sialyl acceptors, which underwent α-(2→4)- and α-(2→8)-sialylation in good yield. In this paper, we report the successful use of 1,5-lactamized sialyl units in the production of α-(1→4)- and α-(1→8)-fucosyl sialic acid sequences, which are substructure of complex gangliosides HPG-7 and HPG-1, respectively.

2. Results and discussion

Recently, Higuchi's group identified the novel gangliosides HPG-1[5] and HPG-7[6] from the sea cucumber

☆ Part 140 of the series: synthetic studies on sialoglycoconjugates. For Part 139 see Ref. 4.

* Corresponding authors. Tel./fax: +81 58 293 2617 (H.A.); e-mail: hando@cc.gifu-u.ac.jp

0008-6215/$ - see front matter © 2006 Elsevier Ltd. All rights reserved.
doi:10.1016/j.carres.2006.03.017

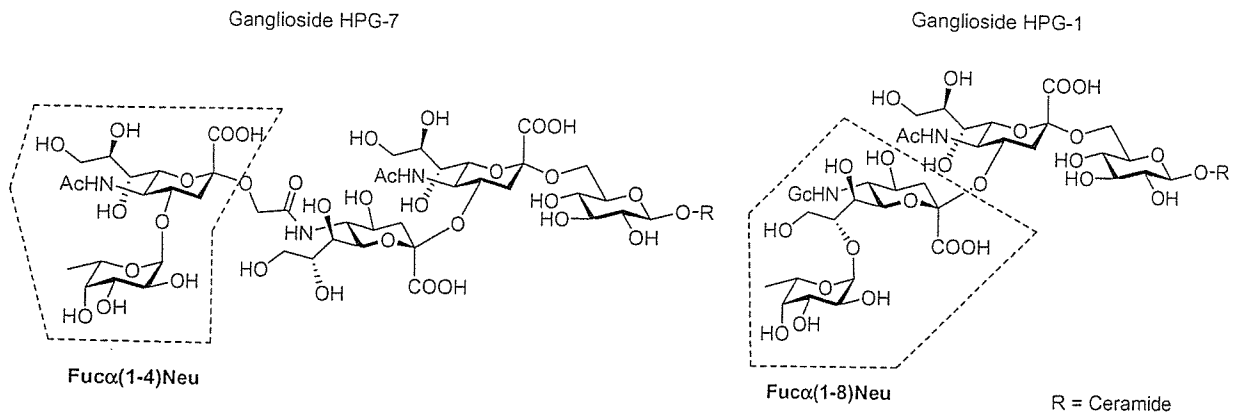

Figure 1. Structures of the HPG-7 and HPG-1 gangliosides.

Holothuria pervicax. These compounds showed neuritogenic activity toward rat pheochromocytoma PC-12 cells and therefore are attracting considerable attention with respect to the development of new compounds for treating neural disease. As shown in Figure 1, the sialic acid termini of HPG-7 and HPG-1 are glycosylated with fucopyranosyl residues through either α-(1→4) or α-(1→8) linkages. Previously, we developed a method to assemble the α-Neu*p*Gc-(2→4)-α-Neu*p*5Ac-(2→6)-Glc*p* sequence based on the combined use of a reactive 1,5-lactamized sialyl acceptor and *N*-(2,2,2-trichloroethoxycarbonyl)-protected sialyl donors.[4] To complete the synthesis of HPG-7 and HPG-1, the construction of α-Fuc*p*-(1→8)-Neu*p* and α-Fuc*p*-(1→4)-Neu*p* sequences remains to be achieved.

2.1. Design and synthesis of acceptors

For the synthesis of the α-Fuc*p*-(1→4)-Neu*p*5Ac substructure, we designed two acceptors, the 4,7-diol sialyl thioglycoside **2** and the 1,5-lactamized sialyl thioglycoside **8**. For the α-Fuc*p*-(1→8)-Neu*p*5Gc sequence, 1,5-lactamized and *N*-trifluoroacetyl (NTFA)-protected sialyl acceptors, **12** and **13**, were chosen. In addition, the N-acetylated (NAc) sialyl acceptor **5** was used to evaluate the effect of the C5 substituent on the reactivity of the C8 hydroxyl group.

From the known sialic acid phenyl thioglycoside, **1**,[7] straightforward chemistry furnished acceptors **2** and **5** (Scheme 1). Thus, treatment of **1** with sodium methoxide followed by dimethoxypropane and camphorsulfonic acid yielded **2** in 60% overall yield, while deacetylation of **1** followed by reaction with benzaldehyde dimethyl acetal and camphorsulfonic acid gave **3** in 77% yield over the two steps. The positions of acetal functionality in **2** and **3** were confirmed to be at C8 and C9 by acetylation of the product, yielding **2′** and **4**. In the ^{1}H NMR spectrum of **2′** and **4**, the signals for the C4 and C7 protons were shifted downfield; for example, comparing **2′** and **2**, the signal for H4 moved to 4.89 from 3.52 ppm, while that for H7 moved to 5.35 ppm from 3.48 ppm. Reductive cleavage of the benzylidene acetal in **4** upon reaction with borane dimethylamine complex and aluminum chloride afforded **5** in 49% yield. The same transformations used to convert **1** into **5** were used (Scheme 2) to synthesize acceptor **13** from the NTFA sialyl thioglycoside **6**,[3] via intermediates **9** and **10** in 65% overall yield.

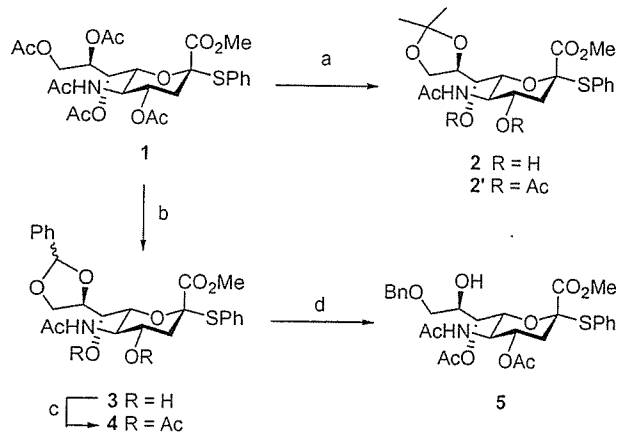

Scheme 1. Preparation of NAc sialyl acceptors. Reagents and conditions: (a) (i) $NaOCH_3$, CH_3OH, rt, 27 h; (ii) 2,2-dimethoxypropane, CSA/CH_3CN, rt, 1.5 h, 60% (two steps); (b) (i) $NaOCH_3$, CH_3OH, rt, 27 h; (ii) $PhCH(OCH_3)_2$, CSA/DMF, 40 °C, 18 h, 77% (two steps); (c) Ac_2O, pyridine, rt, quant.; (d) $BH_3{\cdot}N(CH_3)_2$, $AlCl_3$/THF, 4 Å molecular sieves, 5 h, 0 °C→45 °C, 49%.

In addition, **6** was also the precursor to the 1,5-lactamized acceptors **8** and **13** (Scheme 2). Reaction of **6** with sodium methoxide and then isopropylidenation of the resulting tetrol yielded an 71% yield of **7**, which was then converted to lactam **8** in 99% upon treatment with sodium methoxide at reflux for 4 days. Similarly, lactam formation from **9** afforded **11**, which was then acetylated in 94% overall yield. The benzylidene acetal in **11** was reductively opened upon treatment with borane dimethylamine complex and aluminum chloride[8] yielding **12** in 74% yield.

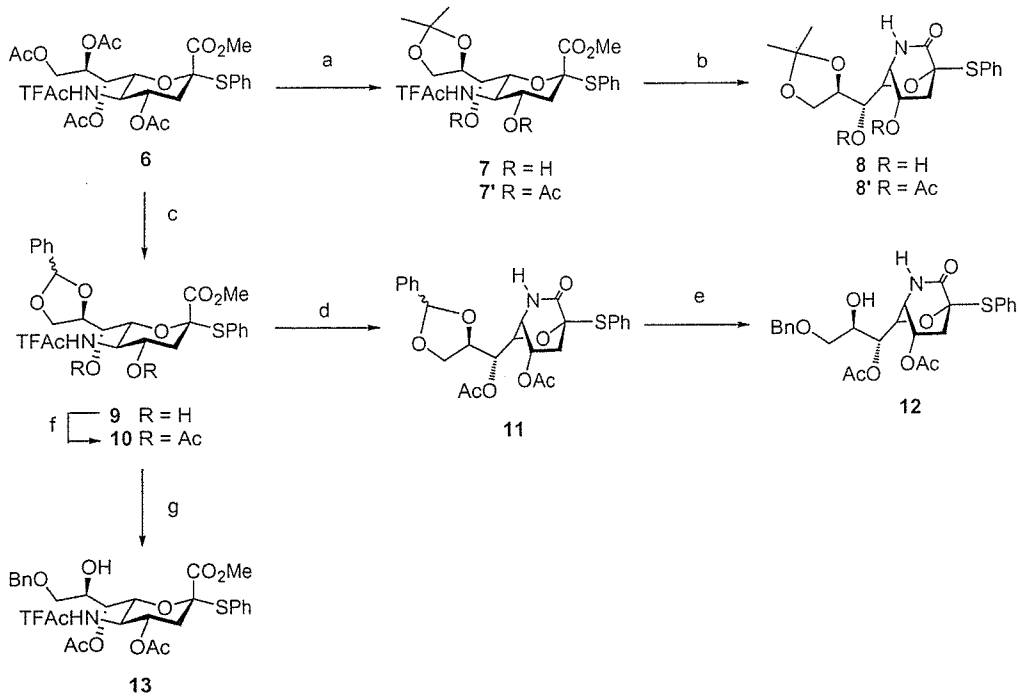

Scheme 2. Preparation of sialyl acceptors. Reagents and conditions: (a) (i) $NaOCH_3$, CH_3OH, rt, 24 h; (ii) 2,2-dimethoxypropane, CSA/CH_3CN, rt, 7 h, 71% (two steps); (b) $NaOCH_3$, CH_3OH, Drierite, reflux, 4 days, 99%; (c) (i) $NaOCH_3$, CH_3OH, rt, 29 h; (ii) $PhCH(OCH_3)_2$, CSA/DMF, 40 °C, 2 h, 88% (two steps); (d) (i) $NaOCH_3$, CH_3OH, Drierite, reflux, 5 days; (ii) Ac_2O, Py, DMAP, rt, 3 h; (iii) NH_2NH_2·AcOH/THF, rt, 80 min, 94% (three steps); (e) BH_3·$N(CH_3)_2$, $AlCl_3$/THF, 4 Å molecular sieves, 6 h, 0 °C→rt, 74%; (f) Ac_2O, pyridine, rt, quant.; (g) BH_3·$N(CH_3)_2$, $AlCl_3$/THF, 4 Å molecular sieves, 3 h, 0 °C, 74%.

2.2. Glycosylation reactions

We initially glycosylated acceptors **2** and **8** (1.0 equiv each) with fucosyl donors **14**[9] and **15**[9] (1.2 equiv each) as shown in Scheme 3. For **2**, the fluoride donor **14** was selected as an orthogonal coupling partner.[10] Among various activation systems for fluoride donors, the use of the Suzuki method[11] (Cp_2HfCl_2/AgOTf) and 2,6-lutidine as an acid scavenger successfully activated fucosyl donor **14** in CH_2Cl_2 at −40 °C to rt without destroying the 8,9-*O*-isopropylidene moiety of **2**, thus producing the α-(1→4)-fucosyl sialoside in 40% yield as a α/β-mixture. However, the α- and β-isomers were inseparable by silica gel column chromatography. For the 1,5-lactamized acceptor **8**, thioglycoside **15** could serve as the donor due to the inactive phenylthio group on the bridge-head carbon of **8**.[4] The coupling reaction between **8** and **14** produced a complex mixture, which was acetylated to facilitate chromatographic separation. For this reaction disaccharide **17** was obtained in a yield of 45% as an α/β-mixture, together with the β-(2→7)-fucosyl disaccharide **18** (8%) and the double fucosylated product **19** (4%). The structure of product **19** was based on mass spectroscopic analysis. This compound showed a peak at $m/z = 1236.56$ in the MALDI MS spectrum, which corresponds to the $[M+Na]^+$ adduct (calculated for $C_{72}H_{79}NO_{14}S = 1236.51$). In contrast, donor **15** was regio- and stereoselectively glycosylated **8** upon activation with *N*-iodosuccinimide (NIS) and trifluoromethanesulfonic acid (TfOH)[12] to produce **17** in 48% yield, accompanied with slight amount of the β-isomer (7%).

The poor stereoselectivity observed in the reaction of the NAc-containing acceptor **2** and donor **14** was seen in the glycosylation of another NAc-containing acceptor, **5** (Scheme 4). In addition, the reaction of **5** and **14** provided an α/β mixture that was inseparable. Fortunately, a better result was obtained in the reaction of the NTFA-protected acceptor **13** with fucosyl donor **14**. This glycosylation furnished the α-Fuc*p*-(1→8)-Neu*p* sequence, with the α-anomer predominating, but chromatographic separation was again demanding. In contrast, fucosylation of the 1,5-lactamized-8-hydroxy acceptor **12** with donors **14** and **15** successfully delivered disaccharides. In both cases, although the stereoselectivity was moderate, anomer separation was readily achieved to afford pure α- and β-glycosides (Scheme 4). Overall, these results show that the 1,5-lactamized acceptors **8** and **12** are the best acceptors in α-(1→4)- and α-(1→8)-fucosylations, respectively. The stereochemistry of all glycosylations was determined from $J_{1,2}$ coupling constants in ^1H NMR spectra of the products (for the α-glycosides $J_{1,2} = 3.3$–4.0 Hz and for the β- glycosides: $J_{1,2} = 7.6$–10.5 Hz).

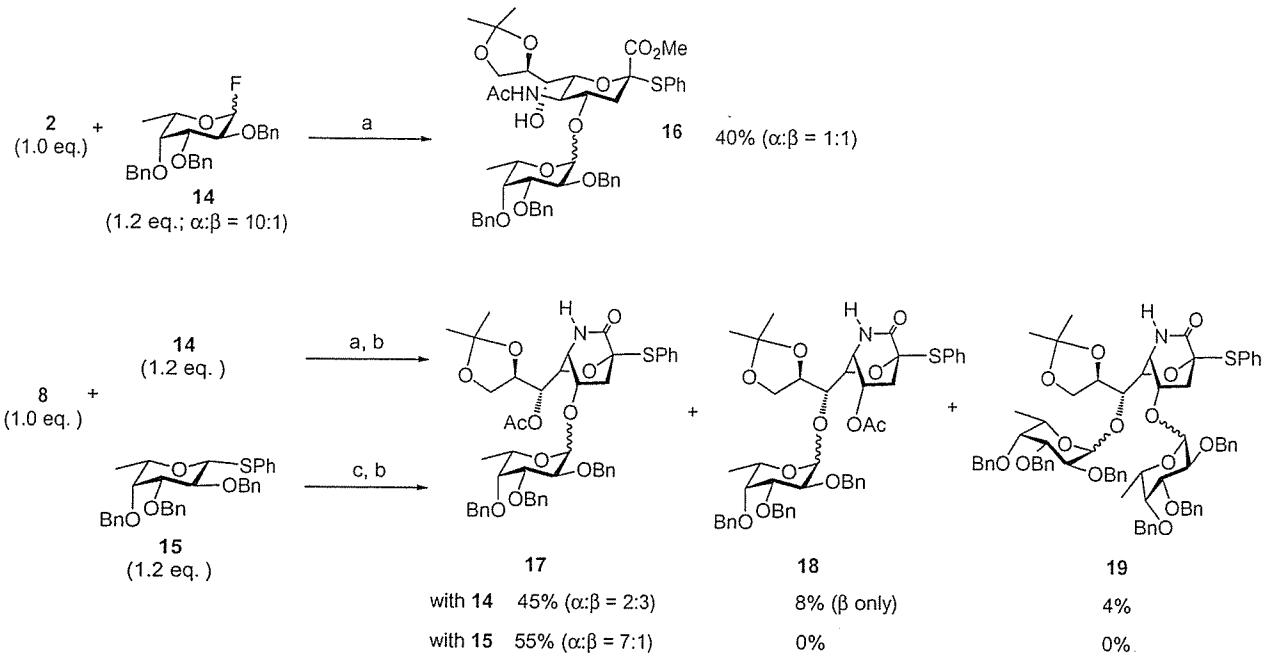

Scheme 3. Examination of α-(1→4)-fucosylation of sialic acid acceptors. Reagents and conditions: (a) Cp_2HfCl_2, AgOTf, 2,6-lutidine/CH_2Cl_2, 4 Å molecular sieves, −80 °C→− 10 °C; (b) Ac_2O, pyridine; (c) NIS, TfOH/CH_2Cl_2, 4 Å molecular sieves, −40 °C, 5 min.

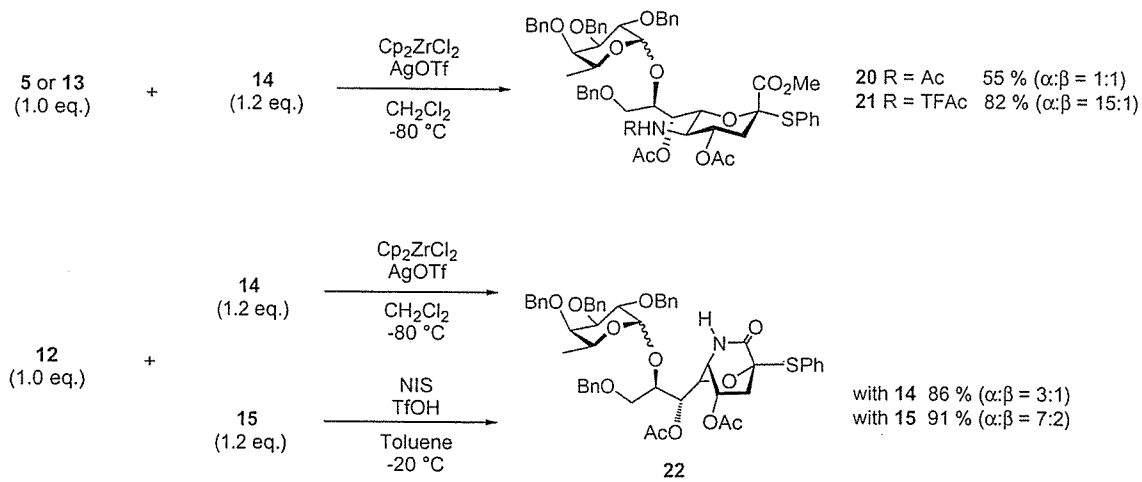

Scheme 4. Examination of α-(1→8)-fucosylation of sialic acid acceptors.

Finally, the protected α-Fuc*p*-(1→8)-Neu*p* derivative bearing 1,5-lactam ring (**22**) was transformed into an active disaccharide glycosyl donor by following the protocol developed[4] for the α-Neu*p*-(2→8)-Neu*p* structural motif (Scheme 5). Thus, the benzyloxycarbonyl (Cbz) group was installed onto the amide moiety yielding an 92% yield of **23**, which was then subjected to alkaline hydrolysis and methylation with methyl iodide, thereby providing disaccharide donor **24** in 92% yield over the two steps.

2.3. Conclusions

In conclusion, for the α-(1→4)- and α-(1→8)-fucosylation of sialic acid, 1,5-lactamized derivatives **8** and **12** serve as highly reactive glycosyl acceptors as was demonstrated in the case of α-(1→4)- and α-(1→8)-sialylations. The excellent results obtained from the coupling of NTFA-protected acceptor **13** support earlier observations made by the Boons' group,[13] which showed that the reactivity of the C8 hydroxyl group is increased when a trifluoroacetate group protects the C5 amino group.

To the best of our knowledge, this is the first report on the fucosylation of sialic acid. We note that in spite of the high reactivity of fucosyl donors as shown by many oligosaccharide syntheses,[9,14] the attachment of fucose to the C4 and C8 positions of sialic acid requires the use of optimized sialyl acceptors. These results suggest

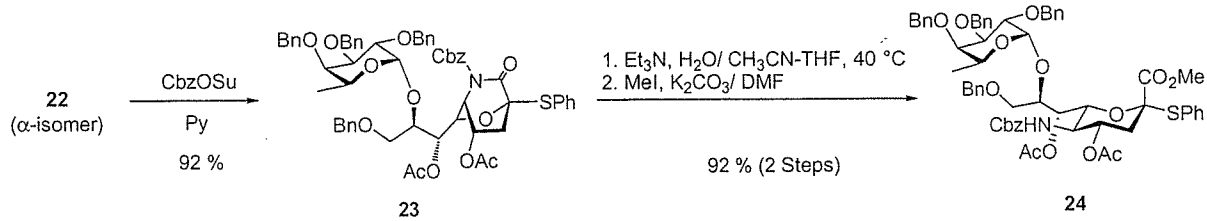

Scheme 5. Transformation of **22** into disaccharide donor **24**.

that, with the exception of the primary C9 hydroxyl group, the other hydroxyl groups in sialic acid are inherently poorly reactive. In this context, the 1,5-lactamized acceptor should also be of use for other glycosyl modifications of sialic acid residues found in nature, including those linked to galactose[1b] and galactosamine[15] residues. In preliminary studies, we have succeeded in the synthesis of the tetrasaccharide portion of HPG-1 by use of donor **24**. This result of this study will be reported in the near future.

3. Experimental

3.1. General procedures

^{1}H and ^{13}C NMR spectra were recorded on Varian Unity INOVA 400, 500 and Jeol ECA 500 instruments. Chemical shifts are expressed in parts per million (δ) relative to the signal of either $CHCl_3$ or $(CH_3)_4Si$, adjusted to 7.26 or 0.00 ppm, respectively. MALDI-TOFMS spectra were recorded in positive ion mode on a Brucker Autoflex with the use of α-cyano-4-hydroxy-cinnamic acid (CHCA) as a matrix. Molecular sieves were purchased from Wako Chemicals Inc. and dried at 300 °C for 2 h in a muffle furnace prior to use. Drierite was powdered and dried at 300 °C for 6 h in a muffle furnace prior to use. Reaction solvents were dried over molecular sieves and used without purification. TLC analysis was performed on Merck TLC (Silica Gel $60F_{254}$ on glass plates). Silica gel (80 mesh and 300 mesh) manufactured by Fuji Silysia Co. was used for flash column chromatography. The quantity of silica gel was usually estimated as 100- to 150-fold weight of sample to be charged. Solvent systems in chromatography are specified in v/v. Evaporation and condensations were carried out in vacuo.

3.2. Methyl (phenyl 5-acetamido-3,5-dideoxy-8,9-*O*-isopropylidene-2-thio-D-*glycero*-α-D-*galacto*-2-nonulopyranosid)onate (2)

To a solution of methyl (phenyl 4,7,8,9-tetra-*O*-acetyl-5-acetamido-3,5-dideoxy-2-thio-D-*glycero*-α-D-*galacto*-2-nonulopyranosid)onate (**1**, 5.00 g, 8.57 mmol) in CH_3OH (170 mL), a 28% solution of sodium methoxide in CH_3OH (166 mg, 0.86 mmol) was added under argon. The mixture was stirred for 27 h at rt, with monitoring of the reaction by TLC (5:1, $CHCl_3/CH_3OH$). The reaction mixture was neutralized with Dowex HCR-W2-H(H^+), filtered, and concentrated. The resulting residue was dried in vacuo, dissolved in CH_3CN (171 mL) and warmed to 40 °C. To the solution, 2,2-dimethoxypropane (1.58 mL, 12.9 mmol) and ±10-camphorsulfonic acid (99.5 mg, 42.8 μmol) were added. The mixture was stirred for 1.5 h at ambient temperature until the starting material was disappeared by TLC (5:1, $CHCl_3/CH_3OH$). The reaction mixture was alkalized to pH ~ 9 with Et_3N and co-evaporated with toluene. The residue was purified by column chromatography on silica gel (25:1, $CHCl_3/CH_3OH$) to give **2** (2.35 g, 60%): $[\alpha]_D$ −0.05 (*c* 0.1, $CHCl_3$); ^{1}H NMR (400 MHz, $CDCl_3$): δ 7.42–7.27 (m, 5H, 2Ph), 6.27 (d, 1H, NH), 4.19 (m, 1H, H-8), 4.14 (dd, 1H, $J_{8,9} = 6.2$ Hz, $J_{gem} = 8.4$ Hz, H-9), 3.95 (dd, 1H, $J_{8,9'} = 7.0$ Hz, H-9′), 3.85 (q, 1H, H-5), 3.66 (dt, 1H, $J_{3ax,4} = 11.0$ Hz, $J_{3eq,4} = 4.8$ Hz, H-4), 3.50 (s, 3H, Me), 3.47 (m, 1H, H-7), 3.25 (d, 1H, H-6), 2.91 (dd, 1H, $J_{gem} = 12.8$ Hz, H-3eq), 2.01 (s, 3H, NAc), 1.89 (t, 1H, H-3ax), 1.34, 1.24 (2s, 6H, 2Me); ^{13}C NMR (100 MHz, $CDCl_3$): δ 173.2, 169.4, 136.7, 129.9, 129.1, 128.6, 108.6, 87.3, 76.7, 76.6, 74.9, 74.9, 70.3, 70.2, 68.3, 68.1, 67.2, 52.6, 52.5, 52.2, 40.8, 26.7, 25.3, 23.1, 23.1; MALDI-TOFMS *m/z* calcd for $C_{21}H_{29}NO_8S$ $[M+Na]^+$: 478.15. Found 478.02.

3.3. Methyl (phenyl 5-acetamido-4,7-di-*O*-acetyl-3,5-dideoxy-8,9-*O*-isopropylidene-2-thio-D-*glycero*-α-D-*galacto*-2-nonulopyranosid)onate (2′)

$[\alpha]_D$ +1.3 (*c* 0.1, $CHCl_3$); ^{1}H NMR (400 MHz, $CDCl_3$): δ 7.70–7.29 (m, 5H, Ph), 5.40 (d, 1H, NH), 5.29 (dd, 1H, $J_{6,7} = 4.8$ Hz, $J_{7,8} = 1.8$ Hz, H-7), 4.92 (td, 1H, $J_{3ax,4} = 11.0$ Hz, $J_{3eq,4} = 4.8$ Hz, H-4), 4.24 (m, 1H, $J_{8,9} = 6.6$ Hz, H-8), 3.97 (m, 2H, H-9 and H-5), 3.67 (dd, 1H, $J_{5,6} = 1.4$ Hz, H-6), 3.62 (s, 3H, Me), 2.81 (dd, 1H, $J_{gem} = 12.8$ Hz, H-3eq), 2.16–1.86 (m, 10H, H-3 ax, 3Ac), 1.31, 1.29 (2s, 6H, 2Me); ^{13}C NMR (100 MHz, $CDCl_3$): δ 170.9, 170.3, 170.2, 168.5, 136.8, 130.2, 128.8, 128.7, 108.5, 87.5, 75.7, 75.3, 69.5, 69.0,

66.0, 52.7, 49.5, 37.8, 26.4, 25.4, 23.1, 20.9, 20.8; MALDI-TOFMS *m/z* calcd for $C_{21}H_{29}NO_8S$ $[M+Na]^+$: 539.18. Found 539.18.

3.4. Methyl (phenyl 5-acetamido-8,9-*O*-benzylidene-3,5-dideoxy-2-thio-D-*glycero*-α-D-*galacto*-2-nonulopyranosid)onate (3)

To a solution of compound **1** (3.85 g, 6.6 mmol) in CH_3OH (132 mL), a 28% solution of sodium methoxide in CH_3OH (128 mg, 0.66 mmol) was added under an argon atmosphere. The mixture was stirred for 27 h at rt with monitoring of the reaction by TLC (5:1, $CHCl_3/CH_3OH$). The reaction mixture was neutralized with Dowex HCR-W2-H(H^+), filtered, and concentrated. The resultant residue was dried in vacuo, dissolved in DMF (73 mL) and warmed up 40 °C. To the solution, benzaldehydedimethylacetal (1.98 mL, 13.2 mmol) and ±10-camphorsulfonic acid (154 mg, 0.66 mmol) were added and stirring was continued for 18 h at 40 °C until the starting material was disappeared by TLC. The reaction mixture was alkalized to pH ~ 9 with Et_3N and concentrated. The resultant syrup was dissolved in $CHCl_3$, and washed with satd aq $NaHCO_3$, brine, and dried over Na_2SO_4. After concentration, the residue was purified by column chromatography on silica gel (20:1, $CHCl_3/CH_3OH$) to give **3** (2.31 g, 77%); ^1H NMR (400 MHz, $CDCl_3$): δ 7.51–7.20 (m, 10H, 2Ph), 4.21 (m, 1H, $J_{7,8} = 7.0$ Hz, $J_{8,9} = 7.0$ Hz, $J_{8,9'} = 5.1$ Hz, H-8), 4.12 (dd, 1H, $J_{gem} = 8.4$ Hz, H-9′), 3.91 (m, 1H, H-9), 3.71 (m, 1H, H-5), 3.56–3.37 (m, 2H, H-4 and H-7), 3.32–3.30 (m, 4H, H-6 and Me), 2.71 (dd, 1H, $J_{gem} = 12.5$ Hz, $J_{3eq,4} = 4.8$ Hz, H-3eq), 1.85 (s, 3H, 3Ac), 1.69 (t, 1H, $J_{3ax,4} = 11.7$ Hz, H-3ax); ^{13}C NMR (100 MHz, CD_3OD): δ 173.4, 169.1, 137.8, 136.5, 129.6, 129.4, 129.0, 128.4, 127.9, 126.5, 103.8, 87.3, 76.2, 75.9, 69.7, 67.6, 67.5, 52.1, 51.3, 48.3, 48.1, 47.9, 47.7, 47.5, 47.3, 47.1, 40.6, 21.4; MALDI-TOFMS *m/z* calcd for $C_{25}H_{29}NO_8S$ $[M+Na]^+$: 526.56. Found 526.25.

3.5. Methyl (phenyl 5-acetamido-4,7-di-*O*-acetyl-8,9-*O*-benzylidene-3,5-dideoxy-2-thio-D-*glycero*-α-D-*galacto*-2-nonulopyranosid)onate (4)

Compound **3** (2.31 g, 5.1 mmol) was acetylated with Ac_2O and pyridine under conventional conditions to give **4** (2.99 g, quant.); ^1H NMR (400 MHz, $CDCl_3$): δ 7.58–7.27 (m, 10H, 2Ph), 5.35 (dd, 1H, $J_{7,8} = 4.8$ Hz, $J_{6,7} = 2.2$ Hz, H-7), 5.21 (d, 1H, NH), 4.89 (m, 1H, H-4), 4.42 (m, 1H, H-8), 4.17 (dd, 1H, $J_{gem} = 8.4$ Hz, $J_{8,9} = 5.5$ Hz, H-9), 3.99–3.91 (m, 2H, H-5, H-9′), 3.71 (dd, 1H, H-6), 3.52 (s, 3H, Me), 2.80 (dd, 1H, $J_{gem} = 12.8$ Hz, $J_{3eq,4} = 4.8$ Hz, H-3eq), 2.08–1.87 (m, 10H, H-3ax and 3Ac); ^{13}C NMR (100 MHz, CD_3OD): δ 170.7, 170.3, 170.2, 168.5, 137.4, 136.8, 130.2, 129.2, 128.5, 128.3, 126.3, 103.3, 94.3, 87.4, 76.0, 75.6, 70.0, 68.8, 66.8, 52.7, 49.2, 37.8, 23.1, 20.8, 20.8; MALDI-TOFMS *m/z* calcd for $C_{29}H_{33}NO_{10}S$ $[M+Na]^+$: 610.63. Found 610.48.

3.6. Methyl (phenyl 5-acetamido-4,7-di-*O*-acetyl-9-*O*-benzyl-3,5-dideoxy-2-thio-D-*glycero*-α-D-*galacto*-2-nonulopyranosid)onate (5)

To a mixture of compound **4** (251 mg, 0.427 mmol) and 4 Å molecular sieves (1.5 g) in THF (5.0 mL), $BH_3{\cdot}NMe_3$ (193 mg, 2.65 mmol) and $AlCl_3$ (342 mg, 2.56 mmol) were added at 0 °C. The reaction mixture was stirred for 1 h at 0 °C and for another 1 h at rt (TLC; 10:1, $CHCl_3/CH_3OH$). $AlCl_3$ (228 mg, 1.70 mmol) was added to the reaction mixture, and stirred for 2.5 h at rt and for 0.5 h at 45 °C. The reaction mixture was filtered through Celite and the combined filtrate and washings were extracted with EtOAc. The organic layer was washed with satd aq $NaHCO_3$ and brine, dried over Na_2SO_4, and concentrated. The residue was purified by column chromatography on silica gel (50:1, $CHCl_3/CH_3OH$) to give **12** (126 mg, 49%); $[\alpha]_D$ +5.8 (*c* 1.1, $CHCl_3$); ^1H NMR (400 MHz, $CDCl_3$): δ 7.54–7.26 (m, 10H, 2Ph), 5.34 (d, 1H, NH), 5.10 (dd, 1H, $J_{6,7} = 2.2$ Hz, H-7), 4.79 (td, 1H, $J_{3eq,4} = 4.8$ Hz, $J_{3ax,4} = 11.4$ Hz, $J_{4,5} = 10.6$ Hz, H-4), 4.59–4.48 (m, 2H, $PhCH_2$), 4.14 (q, 1H, $J_{5,6} = 10.6$ Hz, H-5), 4.06 (m, 1H, H-8), 3.74 (dd, 1H, H-6), 3.69 (s, 3H, Me), 3.50 (dd, 1H, $J_{gem} = 9.5$ Hz, H-9), 3.42 (dd, 1H, H-9′), 2.86 (dd, 1H, $J_{gem} = 12.8$ Hz, H-3eq), 2.10–2.03 (m, 7H, H-3ax and 2Ac); ^{13}C NMR (100 MHz, CD_3OD): δ 170.8, 170.3, 170.2, 169.3, 138.1, 136.7, 130.5, 128.9, 128.2, 128.0, 127.9, 127.5, 86.5, 75.1, 73.4, 70.8, 70.1, 69.3, 69.3, 53.3, 48.6, 37.3, 30.0, 23.1, 21.0, 20.8; MALDI-TOFMS *m/z* calcd for $C_{29}H_{35}NO_{10}S$ $[M+Na]^+$: 612.64. Found 612.26.

3.7. Methyl (phenyl 3,5-dideoxy-8,9-*O*-isopropylidene-2-thio-5-trifluoroacetamido-D-*glycero*-α-D-*galacto*-2-nonulopyranosid)onate (7)

To a solution of compound **6** (5.34 g, 8.4 mmol) in CH_3OH (100 mL), a 28% solution of sodium methoxide in CH_3OH (162 mg, 0.84 mmol) was added under an argon atmosphere. The mixture was stirred for 24 h at rt, with monitoring of the reaction by TLC (10:1, $CHCl_3/CH_3OH$). The reaction mixture was neutralized with Dowex HCR-W2-H(H^+), filtered, and concentrated. The resultant residue was dried in vacuo, dissolved in DMF (157 mL) and warmed up 40 °C. To the solution, 2,2-dimethoxypropane (1.45 mL, 11.8 mmol) and ±10-camphorsulfonic acid (91 mg, 0.39 mmol) were added and stirring was continued for 7 h at rt until the starting material disappeared by TLC. The reaction mixture was alkalized to pH ~ 9 with Et_3N and concentrated. The

residue was purified by column chromatography on silica gel (2:1, *n*-hexane/EtOAc) to give **7** (2.84 g, 71%); $[\alpha]_D$ −1.0 (*c* 0.2, $CHCl_3$); ^1H NMR (400 MHz, CD_3OD): δ 7.34–7.44 (m, 5H, Ph), 4.62 (d, 1H, NH), 4.14 (m, 1H, H-8), 3.95 (m, 3H, H-5, H-6, and H-7), 3.67 (m, 1H, H-4), 3.58 (dd, 1H, $J_{8,9} = 1.1$ Hz, $J_{gem} = 10.5$ Hz, H-9), 3.47 (s, 3H, Me), 3.44 (m, 1H, H-9′), 2.81 (dd, 1H, $J_{3eq,4} = 4.8$ Hz, $J_{gem} = 12.8$ Hz, H-3eq), 1.80 (t, 1H, $J_{3ax,4} = 11.4$ Hz, H-3ax), 1.30, 1.22 (2s, 6H, 2Me); ^{13}C NMR (100 MHz, CD_3OD): δ 170.2, 137.9, 130.9, 130.5, 129.6, 109.8, 88.6, 76.8, 76.3, 70.7, 68.6, 67.7, 53.5, 52.6, 41.8, 27.0, 25.7, 14.5; MALDI-TOFMS *m/z* calcd for $C_{21}H_{29}F_3NO_8S$ $[M+H]^+$: 477.18. Found 478.34.

3.8. Methyl (phenyl 4,7-di-*O*-acetyl-3,5-dideoxy-8,9-*O*-isopropylidene-2-thio-5-trifluoroacetamido-D-*glycero*-α-D-*galacto*-2-nonulopyranosid)onate (7′)

$[\alpha]_D$ +1.3 (*c* 0.1, $CHCl_3$); ^1H NMR (400 MHz, $CDCl_3$): δ 7.27–7.57 (m, 5H, Ph), 6.47 (d, 1H, NH), 5.20 (dd, 1H, $J_{6,7} = 5.2$ Hz, $J_{7,8} = 1.5$ Hz, H-7), 5.09 (td, 1H, $J_{3eq,4} = 5.1$ Hz, $J_{3ax,4} = 11.4$ Hz, $J_{4,5} = 11.4$ Hz, H-4), 4.28 (dd, 1H, $J_{5,6} = 6.6$ Hz, H-6), 3.94 (m, 3H, H-5, H-8, and H-9), 3.82 (dd, 1H, $J_{8,9'} = 1.5$ Hz, $J_{gem} = 11.1$ Hz, H-9′), 3.62 (s, 3H, Me), 2.87 (dd, 1H, $J_{gem} = 12.8$ Hz, H-3eq), 2.16 and 2.02 (2s, 6H, 2Ac), 1.97 (dd, 1H, H-3ax), 1.32, 1.29 (2s, 6H, 2Me); ^{13}C NMR (100 MHz, $CDCl_3$): 170.9, 170.1, 168.2, 157.7, 157.3, 136.8, 128.8, 128.4, 108.7, 87.5, 74.8, 74.7, 69.1, 68.8, 66.0, 52.8, 50.3, 37.6, 26.3, 25.4, 20.7, 20.6.

3.9. Phenyl 5-amino-3,5-dideoxy-8,9-*O*-isopropylidene-2-thio-D-*glycero*-α-D-*galacto*-2-nonulopyranoside-1,5-lactam (8)

To a solution of compound **7** (2.39 g, 5.0 mmol) in CH_3OH (615 mL), Drierite (6.0 g) and a 28% solution of sodium methoxide were added in CH_3OH (2.8 g, 14.8 mmol) under an argon atmosphere. The suspension was stirred for 4 days at reflux while the reaction was monitored by TLC (5:1, $CHCl_3/CH_3OH$). The reaction mixture was neutralized with Dowex HCR-W2-H(H^+) and filtered through Celite. The combined filtrate and washings were concentrated and the resulting residue was purified by column chromatography on silica gel (15:1, $CHCl_3/CH_3OH$) to give **8** (1.89 g, 99%); $[\alpha]_D$ −6.8 (*c* 0.2, $CHCl_3$); ^1H NMR (500 MHz, $CDCl_3$): δ 7.62–7.28 (m, 5H, Ph), 4.28 (s, 1H, H-6), 4.09 (m, 2H, H-4 and H-8), 3.95 (dd, 1H, $J_{6,7} = 12.8$ Hz, $J_{7,8} = 6.2$ Hz, H-7), 3.78 (near d, 1H, $J_{5,6} = 5.9$ Hz, H-5), 3.67 (m, 2H, H-9 and H-9′), 2.87 (t, 1H, $J_{3eq,4} = 11.0$ Hz, $J_{gem} = 13.9$ Hz, H-3eq), 1.83 (dd, 1H, $J_{3ax,4} = 3.7$ Hz, H-3ax), 1.36, 1.26 (2s, 6H, 2Me); ^{13}C NMR (125 MHz, $CDCl_3$): δ 170.6, 170.5, 136.4, 129.3, 128.8, 109.7, 85.7, 78.3, 76.7, 76.0, 70.4, 67.2, 66.9, 53.7, 53.6, 41.0, 29.6, 26.5, 25.2; MALDI-TOFMS *m/z* calcd for $C_{18}H_{23}NO_6S$ $[M+H]^+$: 382.12. Found 382.16.

3.10. Phenyl 5-acetamido-4,7-di-*O*-acetyl-3,5-dideoxy-8,9-*O*-isopropylidene-2-thio-D-*glycero*-α-D-*galacto*-2-nonulopyranoside-1,5-lactam (8′)

$[\alpha]_D$ +4.7 (*c* 0.1, $CHCl_3$); ^1H NMR (400 MHz, $CDCl_3$): δ 7.58–7.21 (m, 5H, Ph), 5.62 (dd, 1H, $J_{7,8} = 5.9$ Hz, $J_{6,7} = 8.1$ Hz, H-7), 5.31 (dd, 1H, $J_{4,5} = 3.3$ Hz, $J_{5,6} = 1.8$ Hz, H-5), 4.92 (m, 1H, H-4), 4.12 (m, 1H, H-8), 4.07 (dd, 1H, H-6), 4.01 (dd, 1H, $J_{8,9} = 6.2$ Hz, $J_{gem} = 8.1$ Hz, H-9), 3.80 (dd, 1H, $J_{8,9'} = 7.3$ Hz, H-9′), 2.50 (m, 1H, H-3eq), 2.11 (dd, 1H, $J_{3ax,4} = 2.2$ Hz, H-3ax), 2.07 and 2.06 (2s, 6H, 2Ac), 1.38 and 1.34 (2s, 6H, 2Me); ^{13}C NMR (100 MHz, $CDCl_3$): δ 169.5, 169.4, 169.0, 167.2, 136.6, 129.5, 128.8, 128.3, 109.8, 86.8, 74.7, 70.9, 67.4, 65.7, 48.6, 37.9, 29.7, 26.5, 26.2, 25.2, 21.0, 20.8; MALDI-TOFMS *m/z* calcd for $C_{24}H_{29}NO_9S$ $[M+Na]^+$: 530.14. Found 530.44.

3.11. Methyl (phenyl 8,9-*O*-benzylidene-3,5-dideoxy-2-thio-5-trifluoroacetamido-D-*glycero*-α-D-*galacto*-2-nonulopyranosid)onate (9)

To a solution of compound **6** (300 mg, 0.47 mmol) in CH_3OH (9.4 mL), a 28% solution of sodium methoxide in CH_3OH (8.9 mg, 47 μmol) was added under an argon atmosphere. The mixture was stirred for 29 h at rt, while the reaction was monitored by TLC (10:1, $CHCl_3/CH_3OH$). The reaction mixture was neutralized with Dowex HCR-W2-H(H^+), filtered, and concentrated. The resultant residue was dried in vacuo, dissolved in DMF (5.2 mL), and warmed up 40 °C. To the solution, benzaldehydedimethylacetal (141 μmol) and ±10-camphorsulfonic acid (11 mg, 47 μmol) were added and stirring was continued for 2 h at 40 °C until the starting material disappeared by TLC. The reaction mixture was alkalized to pH ~ 9 with Et_3N and co-evaporated with toluene. The residue was purified by column chromatography on silica gel (1:2, *n*-hexane/EtOAc) to give **11** (230 mg, 88%); ^1H NMR (400 MHz, $CDCl_3$): δ 7.55–7.22 (m, 10H, 2Ph), 5.69 (s, 1H, PhC*H*), 3.68 (s, 1H, H-4), 2.88 (m, 1H, H-3ax), 1.91 (m, 1H, H-3eq); ^{13}C NMR (100 MHz, $CDCl_3$): δ 136.8, 134.5, 129.7, 129.0, 128.8, 128.3, 126.2; MALDI-TOFMS *m/z* calcd for $C_{25}H_{26}F_3NO_8S$ $[M+Na]^+$: 580.12. Found 580.35.

3.12. Methyl (phenyl 4,7-di-*O*-acetyl-8,9-*O*-benzylidene-3,5-dideoxy-2-thio-5-trifluoroacetamido-D-*glycero*-α-D-*galacto*-2-nonulopyranosid)onate (10)

Compound **9** (230 mg, 0.41 mmol) was acetylated with Ac_2O and pyridine by conventional means to give **10** (262 mg, quant.): ^1H NMR (400 MHz, $CDCl_3$): δ 7.59–7.34 (m, 10H, 2Ph), 6.24 (d, 1H, NH), 5.84 (s, 1H), 5.22

(dd, 1H, $J_{7,8}$ = 6.6 Hz, H-7), 5.05 (m, 1H, H-4), 4.46 (m, 1H, H-8), 4.16 (dd, 1H, H-9), 4.00–3.85 (m, 3H, H-9′, H-5, and H-6), 3.43 (s, 3H, Me), 2.90 (dd, 1H, H-3eq), 2.22–1.96 (m, 7H, H-3ax and 2Ac); ^{13}C NMR (100 MHz, $CDCl_3$): δ 170.8, 170.6, 170.3, 170.0, 167.6, 136.4, 130.0, 128.9, 87.5, 73.8, 70.1, 69.0, 67.5, 61.8, 52.8, 50.1, 38.0, 20.9, 20.7, 20.6, 20.5; MALDI-TOFMS *m/z* calcd for $C_{29}H_{30}F_3NO_{10}S$ $[M+Na]^+$: 664.14. Found 664.24.

3.13. Phenyl 4,7-di-*O*-acetyl-5-amino-9-*O*-benzylidene-3,5-dideoxy-2-thio-D-*glycero*-α-D-*galacto*-2-nonulopyranoside-1,5-lactam (11)

To a solution of compound **9** (1.59 g, 2.86 mmol) in CH_3OH (300 mL), Drierite (3.4 g) and a 28% solution of sodium methoxide were added in CH_3OH (1.37 g, 7.1 mmol) under an argon atmosphere. The suspension was stirred for 5 days at reflux as the reaction was monitored by TLC (10:1, $CHCl_3/CH_3OH$). The reaction mixture was filtered through Celite, the combined filtrate and washings were concentrated and the residue was purified by column chromatography on silica gel (80:1→70:1→60:1→40:1→5:1, $CHCl_3/CH_3OH$) to give the lactam derivative. To the solution of lactam in pyridine (2.1 mL), Ac_2O (1.62 mL, 17.2 mmol) and 4-dimethylaminopyridine (35.0 mg, 0.286 mmol) were added, and the mixture was stirred for 3 h. The reaction was monitored by TLC (1:2, *n*-hexane/EtOAc). The reaction mixture was co-evaporated with toluene and diluted with EtOAc. The organic phase was washed with 2 M HCl, water, satd aq Na_2CO_3, and brine, dried (Na_2SO_4), and concentrated. The resulting residue was dissolved in THF (57 mL) followed by the addition of hydrazine acetate (264 mg, 2.86 mmol). The mixture was stirred for 80 min at rt, diluted with EtOAc, washed with 2 M HCl, satd aq $NaHCO_3$, and brine, dried (Na_2SO_4), and concentrated. The residue was purified by chromatography on silica gel (1:1, *n*-hexane/EtOAc) to give **11** (1.38 g, 94%): ^{1}H NMR (400 MHz, $CDCl_3$): δ 7.55–7.27 (m, 10H, 2Ph), 5.76 (s, 1H, PhC*H*), 5.72 (m, 1H, H-7), 5.04 (m, 1H, H-4), 3.95 (dd, 1H, J_{gem} = 8.0 Hz, $J_{8,9}$ = 6.6 Hz, H-9), 2.52 (dd, J_{gem} = 14.2 Hz, $J_{3eq,4}$ = 10.6 Hz, H-3eq), 2.14 and 2.05 (2s, 6H, 2Ac); ^{13}C NMR (100 MHz, $CDCl_3$): δ 170.5, 170.4, 169.8, 169.7, 169.3, 169.3, 137.2, 136.4, 136.3, 129.2, 129.2, 128.7, 128.3, 128.2, 128.1, 126.0, 126.0, 104.2, 104.0, 85.7, 79.4, 79.0, 75.6, 74.5, 71.2, 71.1, 68.8, 68.4, 67.8, 66.9, 49.2, 49.1, 37.8, 37.8, 21.0, 20.9, 20.9, 20.5.

3.14. Phenyl 5-amino-4,7-di-*O*-acetyl-9-*O*-benzyl-3,5-dideoxy-2-thio-D-*glycero*-α-D-*galacto*-2-nonulopyranoside-1,5-lactam (12)

To a mixture of compound **11** (82.0 mg, 0.16 mmol) and 4 Å molecular sieves (500 mg) in THF (1.9 mL), $BH_3{\cdot}NMe_3$ (72 mg, 0.99 mmol) and $AlCl_3$ (128 mg, 0.96 mmol) were added at 0 °C, and then the mixture was stirred for 2 h at 0 °C and for another 4 h at rt (TLC; 10:1, $CHCl_3/CH_3OH$). The reaction mixture was filtered through Celite, the combined filtrate and washings were extracted with Et_2O. The organic layer was washed with satd aq $NaHCO_3$ and brine before being dried (Na_2SO_4) and concentrated. The residue was purified with column chromatography on silica gel (60:1, $CHCl_3/CH_3OH$) to give **12** (61 mg, 74%): $[\alpha]_D$ 12.0 (*c* 1.0, $CHCl_3$); ^{1}H NMR (500 MHz, $CDCl_3$): δ 7.55–7.25 (m, 10H, 2Ph), 5.51 (dd, 1H, H-7), 5.00 (m, 1H, H-4), 4.49 (m, 2H, PhCH_2), 4.26 (m, 2H, H-5 and H-6), 3.80 (m, 1H, H-8), 3.51 (dd, 1H, J_{gem} = 9.5 Hz, H-9), 3.36 (dd, 1H, H-9′), 2.46 (dd, 1H, J_{gem} = 14.4 Hz, H-3ax), 2.12 (s, 3H, NAc), 2.05 (dd, 1H, H-3eq), 1.89 (s, 3H, Ac); ^{13}C NMR (100 MHz, $CDCl_3$): δ 170.1, 170.1, 169.9, 137.2, 136.2, 129.0, 128.6, 128.5, 128.4, 128.0, 85.6, 79.4, 77.2, 73.5, 72.1, 70.3, 69.8, 68.6, 49.2, 37.5, 21.0, 20.9; MALDI-TOFMS *m/z* calcd for $C_{26}H_{27}NO_8S$ $[M+Na]^+$: 538.16. Found 538.15.

3.15. Methyl (phenyl 4,7-di-*O*-acetyl-9-*O*-benzyl-3,5-dideoxyl-2-thio-5-trifluoroacetamido-D-*glycero*-α-D-*galacto*-2-nonulopyranosid)onate (13)

To a mixture of compound **10** (2.27 g, 3.5 mmol) and 4 Å molecular sieves (13.6 g) in THF (41 mL), $BH_3{\cdot}NMe_3$ (1.58 g, 21.7 mmol) and $AlCl_3$ (2.8 g, 0.42 mol) were added at 0 °C, and then the mixture was stirred for 3 h (TLC; 10:1, $CHCl_3/CH_3OH$). The reaction mixture was filtered through Celite and the combined filtrate and washings were extracted with EtOAc. The organic layer was washed with satd aq $NaHCO_3$ and brine, dried (Na_2SO_4), and concentrated. The residue was purified by column chromatography on silica gel (100:1, $CHCl_3$/MeOH) to give **12** (1.70 g, 74%): $[\alpha]_D$ +40.6 (*c* 1.1, $CHCl_3$); ^{1}H NMR (400 MHz, $CDCl_3$): δ 7.52–7.25 (m, 10H, 2Ph), 6.69 (d, 1H, NH), 5.08 (dd, 1H, $J_{6,7}$ = 2.2 Hz, $J_{7,8}$ = 8.8 Hz, H-7), 4.90 (m, 1H, H-4), 4.56–4.46 (2d, 2H, PhCH_2), 4.13–4.02 (m, 2H, H-5 and H-8), 3.88 (dd, 1H, H-6), 3.67 (s, 3H, Me), 3.46 (dd, 1H, $J_{8,9}$ = 5.9 Hz, J_{gem} = 10.6 Hz, H-9), 3.36 (dd, 1H, $J_{8,9'}$ = 3.3 Hz, H-9′), 2.92 (dd, 1H, $J_{3eq,4}$ = 4.8 Hz, J_{gem} = 12.8 Hz, H-3eq), 2.09–2.00 (m, 7H, H-3ax and 2Ac); ^{13}C NMR (100 MHz, $CDCl_3$): δ 170.9, 170.3, 170.2, 169.2, 138.2, 137.0, 130.8, 129.2, 128.5, 128.2, 128.1, 127.8, 86.7, 74.6, 73.7, 70.9, 69.6, 69.3, 53.7, 49.9, 37.5, 21.0, 20.7; MALDI-TOFMS *m/z* calcd for $C_{29}H_{32}F_3NO_{10}S$ $[M+Na]^+$: 666.16. Found 666.17.

3.16. Phenyl [5-acetamido-3,5-dideoxy-8,9-*O*-isopropylidene-2-thio-4-*O*-(2,3,4-tri-*O*-benzyl-α-L-fucopyranosyl)-D-*glycero*-D-*galacto*-2-nonulopyranosid]onate (16)

To a solution of **2** (110 mg, 0.22 mmol) and **14** (115 mg, 0.26 mmol) in CH_2Cl_2 (4.8 mL), 4 Å molecular sieves